ISTANBUL TECHNICAL UNIVERSITY ★ GRADUATE SCHOOL OF SCIENCE ENGINEERING AND TECHNOLOGY

TUNNELLING INDUCED PHOTON EMISSION FROM SURFACE/INTERFACE SYSTEMS OF GRAPHENE ON COPPER

M.Sc. THESIS

Hakkı Tunç ÇİFTÇİ

Department of Physics Engineering

Physics Engineering Programme

JUNE 2017

ISTANBUL TECHNICAL UNIVERSITY ★ GRADUATE SCHOOL OF SCIENCE ENGINEERING AND TECHNOLOGY

TUNNELLING INDUCED PHOTON EMISSION FROM SURFACE/INTERFACE SYSTEMS OF GRAPHENE ON COPPER

M.Sc. THESIS

Hakkı Tunç ÇİFTÇİ

509151109

Department of Physics Engineering

Physics Engineering Programme

Thesis Advisor: Assoc. Prof. Dr. Oğuzhan GÜRLÜ

JUNE 2017

İSTANBUL TEKNİK ÜNİVERSİTESİ ★ FEN BİLİMLERİ ENSTİTÜSÜ

TÜNELLEME AKIMIYLA İNDÜKLENEN BAKIR ÜSTÜ GRAFEN YÜZEY/ARAYÜZ SİSTEMLERİNİN FOTON EMİSYONU

YÜKSEK LİSANS TEZİ

Hakkı Tunç ÇİFTÇİ

509151109

Fizik Mühendisliği Anabilim Dalı

Fizik Mühendisliği Programı

Tez Danışmanı: Doç. Dr. Oğuzhan GÜRLÜ

HAZİRAN 2017

Date of Submission : 5 May 2017
Date of Defense : 6 June 2017

To my beloved family…

FOREWORD

I am sincerely thankful to Assoc. Prof. Dr. Oğuzhan Gürlü who has widened my horizon by giving a chance to involve in excellent facilities emerged by his great effort and deep knowledge. I always will owe to him and be aware of how valuable opportunity that I was given.

There is no way to express how much I am grateful to my beloved family. Each one of them has always been enlightening my path whenever I needed, standing behind me whatever I attempted.

I thank every single member of NanoBEEs group who has always been one step further than me. I thank to Berk Zengin for being always helpful, polite and supportive companion during our collaborative work as well as our friendship in private life. Secondly, I owe a very special thanks to Dilek Yıldız for her precious guidance since the first day of mine in the laboratory. I also have to mention that I am very glad to be colleague, roommate and friend with Cem Kıncal for being always thrustworthy. I also thank to H. Altuğ Yıldırım for assistance about control electronics, Mert Taşkın who always lends a hand whenever I required and Umut Kamber for CVD processes and Raman spectrum studies.

Lastly I thank to TUBİTAK for their support with 1003 project with grant number 114F036.

June 2017

H. Tunç ÇİFTÇİ
Physics Engineer

TABLE OF CONTENTS

Page

ABBREVIATIONS

STM	**:**	Scanning Tunnelling Microscope
SPM	**:**	Scanning Probe Microscope
pSTM	**:**	Photon Scanning Tunnelling Microscope
AFM	**:**	Atomic Force Microscope
CVD	**:**	Chemical Vapor Deposition
SP	**:**	Surface Plasmon
LSP	**:**	Localised Surface Plasmon
SPP	**:**	Surface Plasmon Polariton
PE	**:**	Photon Emission
UHV	**:**	Ultra High Vacuum
PIN	**:**	p-type/intrinsic/n-type Combination of Semiconductors
V_{LJ}	**:**	Lennard-Jones Potential
VIS	**:**	Visible
NIR	**:**	Near Infrared
2DEG	**:**	Two Dimensional Electron Gas
PMMA	**:**	Polymethyl Methacrylate
3D	**:**	Three Dimensional
DI	**:**	Deionised
AP	**:**	Atmospheric Pressure
LP	**:**	Low Pressure

SYMBOLS

G	**:**	Graphene
Ag	**:**	Silver
Au	**:**	Gold
Cu	**:**	Copper
Al	**:**	Aluminium
PtIr	**:**	Platinum Iridium
Si	**:**	Silicon
GaAs	**:**	Gallium Arsenide
ITO	**:**	Indium Tin Oxide
SiO_2	**:**	Silicon Oxide
d	**:**	Plane Distance
ε	**:**	Error rate
CH_4	**:**	Methane
C	**:**	Carbon
H	**:**	Hydrogen
Ar	**:**	Argon
$FeCl_3$	**:**	Iron (III) Chloride
PMMA	**:**	Polymethyl Methacrylate
w	**:**	Frequency
f	**:**	Frequency
λ	**:**	Wavelength
φ	**:**	Phase
mm	**:**	Millimetre
µm	**:**	Micrometre
nm	**:**	Nanometre
Å	**:**	Angstrom
°C	**:**	Degree Celsius
s	**:**	Second
min	**:**	Minute
sccm	**:**	Standard cubic centimetres per minute
Ar	**:**	Argon
l	**:**	Litre
V	**:**	Volts
pV	**:**	Picovolts
A	**:**	Amps
nA	**:**	Nanoamps
W	**:**	Watt
fW	**:**	Femtowatt

LIST OF TABLES

Page

LIST OF FIGURES

Page

TUNNELLING INDUCED PHOTON EMISSION FROM SURFACE/INTERFACE SYSTEMS OF GRAPHENE ON COPPER

SUMMARY

Imaging with the smallest order of magnitude has always been an essential topic for researchers working in various areas. Especially with the invent of Nobel Prize winner scanning probe microscopy (SPM), investigations in nanoscopic scales have been performed in terms of topographic, electronic, magnetic and optical properties. In this thesis, we have focused on electronic and optical properties of surfaces using photon scanning tunnelling microscopy (pSTM).

Light emission from a planar junctions such as Metal-Insulator-Metal systems attracted noticeable attention. These studies have indicated that surface plasmons are the dominant mechanism of this light emission. Surface plasmons has been defined as collective oscillations delocalised electrons which propagate electromagnetic waves along the conducting surfaces. There might occur different modes of surface plasmons e.g. surface plasmon polariton (SPP) and localised surface plasmon (LSP). SPP defines surface plasmons which are propagating electromagnetic waves along the surface. LSPs are the charge oscillations in the gap plasmons. However, it was also reported that SPPs might be arise by LSPs as well.

With the invent of scanning tunnelling microscopy (STM), photon emission from tunnel junction was applied in nanoscopic scales as well. Photon emission investigations have been performed on surfaces such as noble metals, molecule adsorbed metals, thin film combinations *etc.*with pSTM systems. Although some allotropes of carbon have been investigated in pSTM studies, graphene has not been stated yet in these investigations. In our work, we have focused on photon emission characteristics of chemical vapour deposition (CVD) grown graphene/copper structure.

Graphene is a promising two dimensional material having honeycomb lattice. Several studies have revealed its extraordinary electronic, mechanical and optical properties. On the other hand, graphene can protect where it covers like a shield against exposing to corrosion. In our study performed under ambient conditions, graphene protects copper substrate from oxidation. Certainly the electronic properties of copper has be considered in this investigation.

In this work, photon emission from metal-tunnel junction-graphene/metal system under ambient conditions was first reported. It was clearly seen that crystal orientation of copper facets has a dominant role on this tunnelling induced luminescence from Graphene/Cu sample. Based on measurements, it was determined that the occurrence of free electron surface state of Cu(111) surfaces are decisive in photon emission.

TÜNELLEME AKIMIYLA İNDÜKLENEN BAKIR ÜSTÜ GRAFEN YÜZEY/ARAYÜZ SİSTEMLERİNİN FOTON EMİSYONU

ÖZET

Görüntüleme çözünürlüğü, malzemelerin fiziksel özelliklerini incelenmesi hususunda kritik bir öneme sahiptir. Bu amaçla ölçüm cihazlarının hep daha yüksek çözünürlüklere çıkartırılması, araştırma konuları içerisinde her zaman önemli bir yere sahip olmuştur. Daha sonraları Nobel ödülüne layık görülen taramalı uç mikroskopisi yüzey incelemelerinde görüntüleme çözünürlüğünü atomik mertebelere indirerek çığır açmıştır.

Taramalı uç mikroskopisinin en eski üyesi olan taramalı tünellemeli mikroskopi, 1 Å'dan bile daha düşük mertebelerde iletken ve yarı iletken yüzeylerde morfolojik görüntüleme kapasitesine sahiptir. Bunun yanısıra tünellenen elektronların kontorlünün de kullanıcıda olması spektroskopik ölçümlerin de önünü açmıştır.

Tünelleme elektronları ve örnek yüzey elektronlarının etkileşiminden kaynaklanan bir çok farklı etki de gözlemlenmiştir. Tünelleme elektronları TTM ucundan örnek yüzeyine geçerken yaptıkları foton emisyonu buna güzel bir örnek teşkil eder. Üstelik bu ışıma karakteristiği, atomik çözünürlükteki yüzey topoğrafyası ile eş zamanlı olarak gözlenebilmektedir.

TTM ucu-vakum/hava bariyeri/iletken yüzey geometrisindeki ışımayı incelemeden önce iletken yüzeylerindeki yük yoğunluklarına daha yakından bakmak yerinde olacaktır. Yüzey plazmonları, yüzeyde parallel olarak yayılım gösteren elektromanyetik dalgaları oluşturan serbest yüzey elektronlarının kolektif osilasyonları olarak tanımlanmaktadır. Bu salınımlar uygun koşullarda optik frekanslarla örtüşen elektromanyetik dalgalar oluşturmakta ve bunun sonucunda ışıma görülebilmektedir. Lokalize yüzey plazmonları (LYP) ve yüzey plazmon polaritonları (YPP) ismi verilen özel durumlara mahsus mekanizmalar da mevcuttur. *Yüzey plazmonu* genel olarak yüzey yüklerinin osilasyon hareketini tanımlarken *polariton* YPP arayüzde oluşan elektromanyetik dalgaları belirtmektedir. LYP mekanizmaları ise TTM-ucu ve yüzey kavitesindeki yük dalgalanmalarının oluşturdğu, geçit plazmonları da denilen yapılardır. Bu iki yapı kimi zaman birbirlerinin ortaya çıkmasını da tetikleyebilmektedir.

Farklı gerilimler uygulanan parallel iletken plakalar arasına çeşitli yalıtkan materyaller konularak oluşturulan jonksiyonlardan ışıma gözlemlendiğinde henüz taramalı uç mikroskopları icat edilmemişti. Bu ışımaların fiziksel altyapısını anlamak amacıyla Metal-oksit-metal yapıları kullanılarak detaylı çalışmalar yürütülmüştür. Lamb ve McCarthy, tünelleme elektronlarının jonksiyon üzerinden geçerken yüzey yükleri ile esnek olmayan çarpışma yaparak optik frekanslar ile eşleşebilecek osilasyonlara sebep olduklarını çalışmalarında belirtmişlerdir.

Taramalı uç mikroskoplarının farklı uygulamalar için kullanılmaya başlanmasıyla birlikte, bu ışıma karakteristikleri nano boyutta incelenmeye başlanmıştır. Bu amaçla geliştirilen TTM sistemlerine ise foton taramalı tünellemeli mikroskopu (fTTM) ismi verilmiştir.

fTTM alanındaki çalışmalar, tünelleme akımından kaynaklı foton çıkışını kompleks bir şekilde ele almıştır. Yüzeydeki en ufak yapısal ve kimyasal değişikliğin dahi yüzeydeki yüklerinin karakteristiğini değiştirmesinden ötürü foton emisyonu morfolojiye direk olarak bağlıdır. Diğer bir yandan TTM ucunun kör olması ya da korozyona uğraması da jonksiyon stabilitesini radikal olarak değiştireceğinden ışıma üzerinde etkisi ciddi boyutlardadır. Bu parametreleri göz önünde tutarak, TTM jonksiyonlarından foton çıkışı LYP ve/veya YPP mekanizmalarının yüzey özelliklerine bağlılıkları açısından açıklanmıştır.

Soy metallerin haricinde farklı sistemler de fTTM ile incelenmiştir. Metal yüzeylerinde çeşitli moleküller biriktirilmesiyle ya da farklı ultra ince film kombinasyonlarından oluşan yapılar da bu araştırmalara dahil edilmiştir. Her ne kadar C_{60} gibi farklı allotropları ile kaplı yüzeyler direkt olarak fTTM ölçümlerine dahil edilmiş ise de, bugüne kadar grafen kaplı soy metal sisteminin fTTM çalışması literatürde yer almamaktadır. Bir takım lüminesans çalışmalarına dahil edilmiş olan ve hızla değişik uygulamalara dahil edilen grafenin çarpıcı özelliklerine bir göz atmak gerekir.

Nanotüp, C_{60}, elmas ve grafit son yıllarda bir çok uygulamada sıkça kullanılan karbon alotroplarıdır. Grafen ise Wallace tarafından tek katmanlı grafit ismiyle taktim edilen iki boyutlu karbon kristalidir. Her karbon atomu üç adet bağ kurarak bal peteği örgüsü biçimiyle kristal örgüsünü oluşturur. Grafenin sıradışı yüzey elektroniği, %98'e varan optic geçirgenliği ve aly katmanları korozyona karşı koruyan kararlı yapısı ile yepyeni araştırma konularının açma potansiyeli Nobel ödülünü de beraberinde getirmiştir. Örneğin bakır üzerinde kimyasal buhar biriktirme yöntemi ile büyütülen grafen atmosferik koşullarda dahi alt katmanları korozyona karşı korur. Sadece vakum şartlarında yapılabilen bir çok çalışmanın atmosferik koşullarda da gerçekletirilmesi, günlük kullanıma uygulamalarına yönelik bir çok yeni araştırma alanına öncülük etmiştir.

Bu özelliklerin keşfi için grafen ve alakalı yapıların karakterizasyonu çok büyük önem arz eder. Bu yüzden yaygın olarak büyütülen grafen filmin saflığı, tek ya da çok katmanlı oluşu gibi özellikleri taramalı uç mikroskopisi uygulamalarına başlamadan Raman spektroskopi tekniği ile künyelendirilir. Bu aşamadan sonraki adım taramalı uç teknikleri ile yüzey nano boyutlarda incelenmektedir.

Atomik kuvvet mikroskopu (AKM) sayesinde tarama yüzeyleri herhangi bir elektronik etkiye maruz kalmadan bağımsız olarak belirlenebilmektedir. Çalışmamızda da TTM ölçümlerinden önce mutlaka geniş alanlı AKM incelemeleri ile karakterizasyonu yapılmıştır. Ardından TTM ile yapılan yüzey çalışmalarında atomik çözünürlüklü bal peteği örgüsünden Moire deseni gibi süper periyodik yapılara kadar bir çok özellik atmosferik koşullar altında gözlemlenmiştir. Bunun yanında grafenin altında yer alan bakır kristalinin atomik basamakları analiz yapılabilecek kalitede gözlemlenebilmektedir.

fTTM çalışmalarının fiziksel altyapısı hakkında yeterli bilgi edindikten sonra, grafen yüzey karakterisyonunun da oldukça güvenilir sonuçlar vermesi, grafen yüzeylerinin nano boyutta foton emisyonunun muhtemel sebeplerini incelemeye teşvik etti. Bu doğrultuda

farklı TTM iğne materyalleri ve TTM ucu hazırlama tekniklerininin karşılaştırılmasıyla optimize edilerek çalışmalara başlanmıştır.

Foton emisyonuna sebep olacak şekilde LYP ve YPP uyarılması amacıyla TTM öçümlerine nazaran yüksek tünelleme akımı ve voltaj seviyelerinde çalışılmaktadır. Bu doğrultuda, yüzey karakterizasyon çalışmasının ardından üzerinde grafen/bakır fTTM sisteminin tünelleme akımı ve voltaj değeri yükseltildi. Toporafya, düşük akım ve voltaj değerlerindeki gibi yüksek kalitede sonuçlar verirken, foton haritası açıkça foton çıkışını göstermiştir. En çok dikkat çeken detay ise foton haritasındaki ışıma olan ve olmayan bölgelerin topoğrafya ile uyumlu oluşuydu. Aralarındaki olası bir ilişkiyi ortaya çıkartmak amacıyla çeşitli bölgelerde küçük analiz alanları seçilererek sonuçlara ulaşıldı.

Atomik basamak yükseklikleri ölçülerek rristal yönelimleri, yani Miller indisleri belirlenmiş ve dikkat çekici sonuçlara ulaşıldı. Işıma görülen bölgeler (111) yönelimine sahip iken diğer bölgeler (110) ya da (100) yönelimlerine sahip olduğu saptanmıştır. Bakır kristalinin farklı yönelimlerinin elektronik yapılarında da değişikler görüldüğü teorik olarak bir çok çalışmada açıklanmıştır. Serbest elektron benzeri yüzey enerji seviyelerine sahip olan (111) yönelimleri, aynı şekilde foton çıkışı olan bölgeler olarak dikkat çekmiştir. Çalışmalarımızın ortaya koyduğu bu sonucu, (111) yönelimli yüzeylerin sahip olduğu ayırdedici elektronik özellik sayesinde geçit plazmonlarının YPP'lerin oluşumu tetiklemesi ve foton çıkışını sağladığı şeklinde yorumlanmıştır.

Sonuç olarak karbonların çok özel bir örgüsü olan grafen ile günlük uygulamalarda dahi çok fazla kullanılan bakırın bu kombinasyonu, atomik boyutlarda ışık kaynağı özelliğini ortaya çıkartmıştır. Yapılan çalışmada bu olayın kaynakları anlamaya çalışılmış ve bölgesel olarak değişen bakır kristal yönelimlerinin ışımadaki etkisi analizlere dayandırarak ortaya konulmuştur.

1. INTRODUCTION

Optical microscopes can cover imaging only for the areas which are tens of thousands times bigger than interatomic distances. However, surface imaging with the smallest order of magnitude has always been an essential interest area for researchers. To better comprehend physical phenomena of atomic and molecular structures, a Noble prize winner technique has been developed: scanning tunnelling microscopy (STM). The advent of this scanning probe microscopy (SPM) method has paved the way for extensive surface studies in terms of topographic, electronic, magnetic and optical. In this thesis, photon emission characterisation of various surfaces in nanoscopic scales has been performed using photon scanning tunnelling microscope (pSTM). Thus, a literature survey the physical and experimental background of this phenomena such as surface charge characteristics and photon emission investigations are presented in this chapter.

1.1 Surface Plasmons

Photon emission and surface charge oscillations cannot be considered individually regarding this phenomena has been based on surface plasmons in the literature [1]. Surface plasmons has been defined as collective oscillations delocalised electrons which propagate electromagnetic waves along the conducting surfaces. As it was also named as *the inverse photoelectric effect* by Gimzewski [2], free surface electrons may oscillate coupled with optical frequencies [3, 4].

There might occur different modes of surface plasmons *e.g.* surface plasmon polariton (SPP) and localised surface plasmon (LSP). For SPPs, *surface plasmon* defines the motion of surface charges and described by *polariton* describes electromagnetic waves in vacuum or dielectric side [5]. Differently from SPPs, LSPs are the charge oscillations in the STM tip-surface cavity which are also known as gap plasmons [6]. Although they are two different cases of surface plasmons, transition and interaction between LSPs and SPPs have been reported as well. It has also been demonstrated that the decay of LSPs *e.g.* in a

tunnel junction of an STM may yield rise in SPPs [6]. Thus, LSPs and SPPs has to be considered together in photon emission investigations as well.

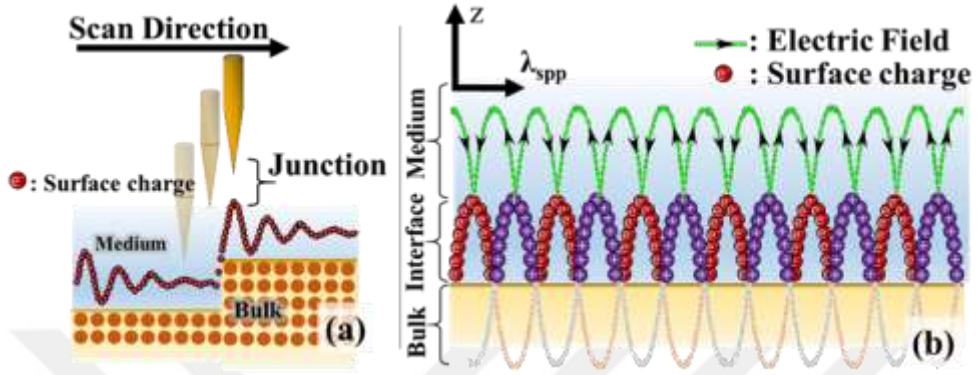

Figure 1.1 : (a, b) Representation of localised surface plasmons (LSP) and surface plasmon polaritons (SPP) respectively.

1.2 Photon Emission from Tunnel Junction

Physical background of photon emission phenomena from planar junctions has to be considered as well which has already been observed before the invention of STM. Occurrence of photon emission in metal-insulator-metal tunnel junctions has been extensively studied. According to Lambe and McCarthy, inelastic excitation yields optically coupled surface plasmon modes in tunnelling junction [7]. They also suggested that surface polariton attenuates roughness-dependently. Photon radiation characteristics in terms of intensity, energy and emission direction angle to the junction normal were also included in several works [8, 9]. These theoretical and experimental investigations based on planar junctions attributed photon emission to surface plasmon polariton (SPP).

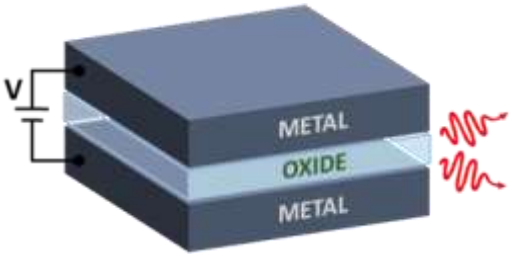

Figure 1.2 : Schematic diagram of photon emission from tunnel junction of Metal-Oxide-Metal (MOM) sandwich.

These inverse photoelectric effect studies paved the way for applying the same phenomena in scanning probe microscopy (SPM) studies. Development of photon scanning tunnelling microscope (pSTM) allowed nanoscopic scaled photon emission investigations with spatial resolution on conductive surfaces.

It was determined that any difference in the material, apex and the cleanness of the tip of a scanning tunnelling microscope (STM) varies emission characteristics individually. STM tip is vertically displaced over the surface by real-time feedback control system by considering tunnelling current at any position. This movement on z-axis directly depends on the local surface electronic properties as well as its morphology. Thus, minute and almost untraceable variance of chemical composition of the surface e.g. oxidation might be decisive in the nature of emitted photons.

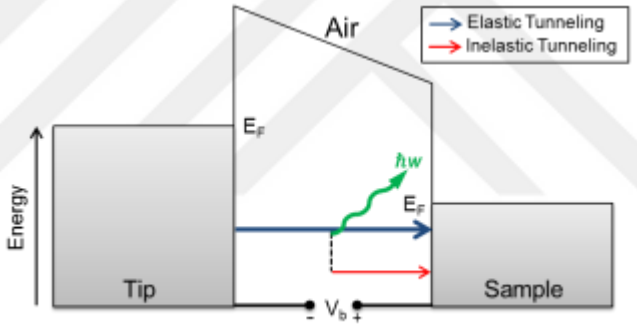

Figure 1.3 : Sketch of inelastic tunnelling and photon emission

In addition to dependency to the surface morphology and chemical composition, further studies have approached to this phenomena from various perspectives. Observation of optical radiation was first originated to local surface plasmon (LSP) which relies on the tip and the surface poles of the junction. In addition, intensity of emitted photon was independent of applied bias voltage as reported by Coombs [1]. For example, the report of Uehara et. al. [10] says the tunnelling current first excites local surface plasmons in the region of tunnelling junction, which was named as direct emission. However, they have also demonstrated the occurrence of photon emission due to some of LSP may decay into surface plasmon polaritons (SPP) in the case of a convenient systems [10, 6]. SPP modes are generated by planar electromagnetic charge waves propagated along two dimensional electron gas over conducting surfaces. Article of Zayats et. al. [11] has presented a detailed theoretical study that contains surface charge oscillation. This study has shown the

mechanisms of LSP waves and SPP waves travelling along metal-vacuum or vacuum-dielectric interfaces.

On the other hand, Persson and Baratoff have revealed equation of LSP in terms of frequency considering suitable boundary conditions of grains [12]. According to their study, inelastic tunnelling has been presented as the dominant mechanism in PE by electron tunnelling to metallic particles. Since the structure of the surface has a manipulative effect on surface plasmons [3], PE may also vary due to surface is tend to emit photons generated by LSPs or SPPs.

1.3 Photon Emission Studies with Photon Scanning Tunnelling Microscope

With the developments of pSTM technique, photon emission have been investigated on surfaces such as noble metals [13] e.g. Ag(111), Au(110), Cu(111) or Si(111) [1] and GaAs [14]. According to these works, occurrence of radiative decays may be in optical (VIS) and near-infrared (NIR) spectra.

There have also been studies about photon emission from different tunnelling junctions such as molecule adsorbed-metal [15-17]. On the other hand, emission mechanism due to interface states has been investigated under different bias voltages [18].

Photon emission from graphene on insulator structure was also investigated by using graphene/ITO/SiO2 sample [19]. Tunnelling induced electroluminescence from graphene due to hot electron luminescence was in infrared region as reported [19, 20].

1.4 Graphene

Different forms of carbon allotropes such as nanotubes [21], fullerene [22], diamond and graphite have been employed in various applications and studies. Graphene was first presented by Wallace in 1947 with the name as “single layer graphite” [23].

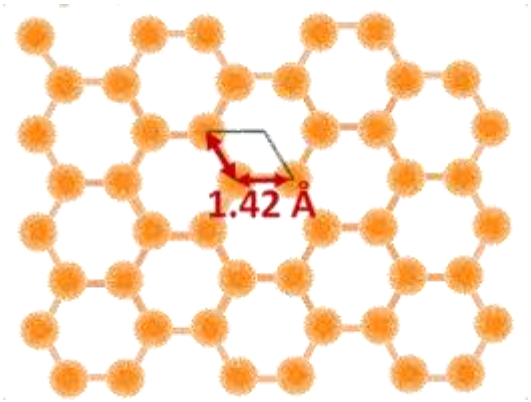

Figure 1.4 : Honeycomb lattice structure of graphene.

In this planar form, there are three bonds per a carbon atom which yields honeycomb crystal shape and unbound electrons. Due to the occurrence of unique electronic, mechanical and optical properties of this hexagonal form, researchers have been studying to better understand and utilise for various applications. Theoretical works about band structure of graphene have revealed charge carriers of graphene in relativistic motion [24, 25]. Moreover, this two-dimensional film has nearly %98 optical transparency which can be observed easily with naked eye [26]. On the other hand, graphene can protect where it covers like a shield against exposing to corrosion [27]. Depending on this protection, some materials which can be oxidised under ambient conditions e.g. copper can be investigated out of vacuum conditions as well. This may open new daily-life applications area by using these easy corrosive materials under ambient conditions with the protection of graphene.

There are two main approaches of photon emission phenomena in a tunnel junction between Graphene/Cu and STM tip and both are based on number of graphene layers. One suggests that increase of number of graphene layers may cause quenching of intensity as Tao has reported [28]. On the other hand, Uehara suggested that refraction index of the produced film may change with number of graphene layers [10]. As a result of this, density oscillation may couple with optical frequencies.

1.5 Free Electron Like Surface States of Specific Metal Facets

Certainly the surface charge properties of the sample as well as LSP and SPP characteristics directly determines the nature of emitted photons. To interpret morphologically changing photon emitting surface plasmons, two dimensional electron gas (2DEG) can be a good example [29, 30].

On the other hand, it has also been known that facet orientation causes variance in electronic band structure as explained by Shockley [31]. According to his study, periodic potentials between atoms in a three-dimensional crystal may have crossed energy bands due to having different lattice constants. Specific surface states might occur as a result of these adjoining bands. In another word, local charge densities of different facets of a crystal might be different. For instance Cu(111) has free electron like states in contrast to Cu(100) [32]. Excitation of free like surface states by tunnelling electrons can yield generation of photon emissive LSPs and SPPs. Thus, photon emissive decays of surface charge oscillation can be attributed to local electronic properties e.g. 2DEG on Cu(111).

Based on this idea, crystal surfaces can be analysed whether local charge characteristics varying with Miller indices are decisive in photon emission. There is a simple method to identify Miller indices by using measured plane heights [33] to understand it there is a relation. If we consider face central cubic copper crystal, lattice constant is 0,361 nm with lattice angles $\pi/2$ each direction. In the given relation (1.1), meaning of a is lattice constant, hkl is Miller indices and d_{hkl} is measured distance between planes respectively.

$$d_{hkl} = \frac{a}{\sqrt{h^2 + k^2 + l^2}} \tag{1.1}$$

$$d_{hkl-multilayer} = n * d_{hkl} \tag{1.2}$$

As a result of lattice plane height calculation, single step height of Cu(111) surface must be 0,208 nm, Cu(100) must be 0,361 nm and Cu(110) must be 0,255 nm. In case of multi-layer terrace occurence as it is shown in Figure.2, orientation can be found approximately by calculating $d_{hkl\text{-}multilayer}$ which is single height constant (d_{hkl}) times number of layer/s (n).

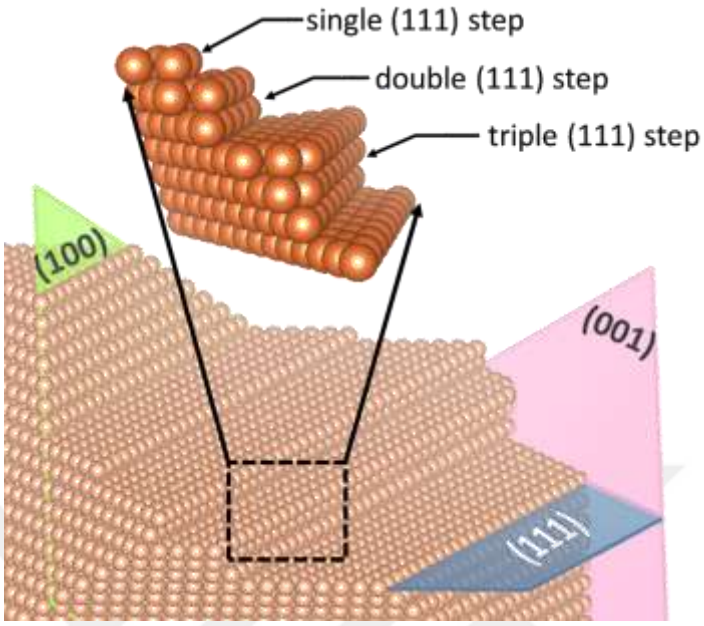

Figure 1.5 : Different orientations of copper crystal and different step characteristics of Cu(111). Measured step height is compared based on the calculations using layer quantity versus crystal orientation. Matching calculated and measured values with the lowest error rate identifies Miller indices.

According to the calculated d_{hkl} values, (111) facet appeared as the smallest among copper crystal orientations. Based on Shockley's claim, this change of interatomic distances might be the reason of free electron like surface states occur where (111) copper facets. Moreover, it has also been known the band diagrams of Cu(100) and Cu(111) are not the same [32].

As a result, we have learned that free electron like surface states should be considered as well in addition to LSP and SPP approaches of photon emission in the literature. Based on that, it is better to identify Miller indices of emissive and non-emissive scan zones whether they are decisive on photon emission or not.

1.6 Purpose of Thesis

Photon STM investigations using Graphene/Cu system can open up new possibilities to study photon emission characteristics of similar surfaces under ambient conditions. Within this study Graphene/Cu have been studied with ambient photon emission scanning tunnelling microscopy (pSTM) and the photon emission from Graphene/Cu system in a

tunnel junction is presented for the first time. Furthermore, a detailed analysis was aimed to be performed based on the approaches of physical background of photon emission mechanisms in a tunnel junction and electronic properties of graphene/copper surface and interface systems.

2. METHODS

2.1 Production and Preparation Methods

2.1.1 Chemical vapour deposition

Different techniques have been developed to grow graphene as mentioned by Novoselov 34. Grain characteristics of the grown graphene which varies as single or multiple graphene layers have always been an important for the ideal growth process. Chemical Vapour Deposition (CVD) appeared as an ideal technique for graphene growth due to scalability on large areas and modifiability of the grain properties and the surface defects [35].

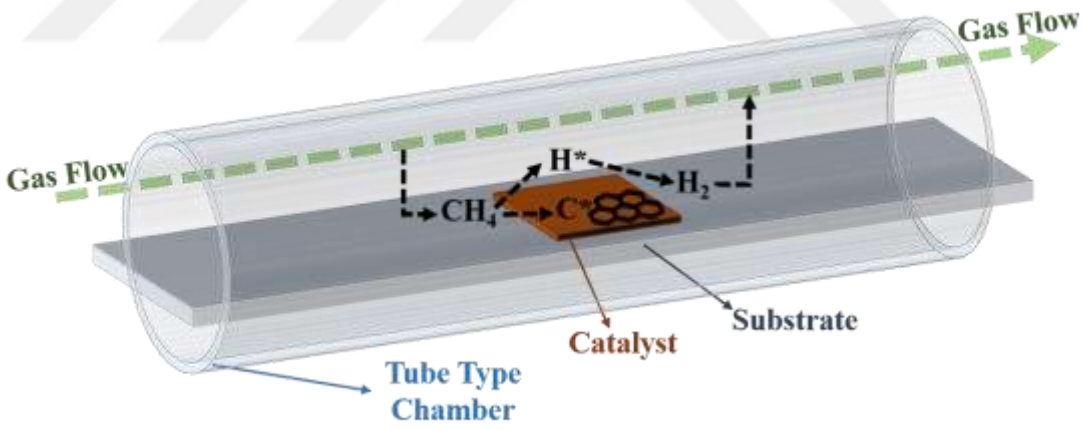

Figure 2.1 : Representation of graphene synthesis during Chemical Vapour Deposition (CVD) process.

In this method, graphene is grown by decomposition of hydrocarbon in gas phase on catalytic metal surfaces. Substrate is heated first and then precursor gases are released into the chamber as represented in Figure 2.1. Based on the conditioning of the reaction chamber, production process can be named as atmospheric pressure CVD (AP-CVD) or low pressure CVD (LP-CVD) [36]. Deposition is processed on the activated surface of the metal substrate due to chemical reactions. Methane (CH_4) diffuses through gas flow and reaches to the substrate surface. Precursor gas decomposes into C and H. Carbon

nucleation occurs in hexagonal form while hydrogen gets exhausted from the chamber with the gas flow [36, 37].

2.1.2 Transfer of graphene on to other substrates

Copper foils have been stated as an ideal substrate for CVD process rather than other wafers due to their low carbon solubility. On the other hand, copper can easily be etched by wet process which is a preferable option. Due to copper substrate can be removed easily, graphene has been transferred on the other substrates as well for different electronic applications. CVD grown graphene layers have been transferred from copper foils on to chosen substrates following a wet chemical procedure using polymethryl-methacrylate (PMMA) [38].

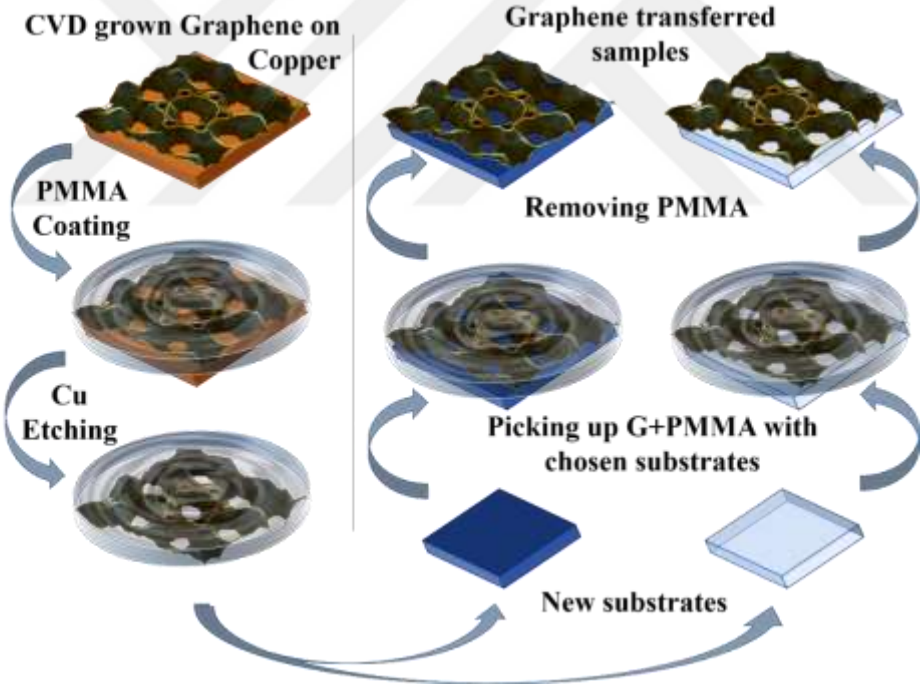

Figure 2.2 : Schematic transfer process of CVD-grown graphene on to dielectric wafers.

2.1.3 Tip preparation and shaping

Photon STM investigations under ambient conditions require tip material which provides the optimum tunnel current stability. Certainly it depends on contamination and the tip shape [39, 40]. It has been known that tungsten or silver needles are used in ultra-high vacuumed (UHV) chambers. However, they are not suitable for ambient conditions due

to tip oxidisation yields significant changes in tunnelling characteristics in a short while. Gold and its alloys have been supplying satisfactory alternatives for ambient conditions as well as PtIr. However, pure Au is the most deformable one in all of these. Although electrochemical etching is the best option for gold tip preparation, this long process may last longer than a stable scan performance of the tip in a junction. Mechanical cut method is another shaping method that is clearly faster and easier process.

$Pt_{80}Ir_{20}$, Au, $Au_{80}Al_{20}$ and homemade $Au_{80}Ag_{20}$ tips were prepared for comparison in terms of preparation process efficiency and stability of the tunnel junction during a scan. The optimised combination was used for all photon emission scanning tunnelling microscopy measurements.

2.2 Measurement Methods

2.2.1 Raman spectroscopy

Raman Spectroscopy is a technique based on inelastic scattering of light which was first predicted by Adolf Smekal [41]. Observation of that effect was presented in the study of Raman and Krishnan in 1928 [42]. The fact that the intensity or *Raman Effect* is approximately 10^{-8} of the incident exciting radiation which requires source stability and intensity. Technologic developments of commercial light sources which became monochromatic, coherent, narrow beam and highly intense have opened a new era in spectroscopy techniques. These sources have been integrated with step motors, photon counting devices, digital acquisition and computer processing. These combinations yielded spectral measurements to be suitable for small scales, coloured samples, solids, liquids, and gases, samples at high temperature, in dilute solutions, under vacuum and in a various conditions. In this work, characterisation of graphene was performed. Using this technique, number of graphene layers was identified on any point of the surface.

Exciting with a radiation yields elastic or inelastic scattering of incident light by atoms or molecules. For a short period, excited molecule stays on virtual energy state until it radiates photon due to relaxation. Inelastic scattering condition results three different cases; elastically scattering by photon retaining incident energy (Rayleigh), or

emitter/scattered photon can be in lower (Stokes) or higher (anti-Stokes) energy level than rovibronic energy state. Rovibronic energy states are defined by interactions between rotational, vibrational and electronic degrees of freedom in a molecule. This measured fluctuation was named as *Stokes Raman shift*, as following expression 2.1 describes in terms of frequency, wavelength and wavenumber [43].

$$\Delta w = \left(\frac{1}{\lambda_0(nm)} - \frac{1}{\lambda_1(nm)}\right) \tag{2.1}$$

However, the unit is commonly chosen as inverse centimetres as given (2.2):

$$\Delta w = \left(\frac{1}{\lambda_0(nm)} - \frac{1}{\lambda_1(nm)}\right) \times \left(\frac{10^7 nm}{cm}\right) \tag{2.2}$$

2.2.2 Scanning tunnelling microscopy

Scanning Tunnelling Microscopy (STM) is an surface investigation technique in atomic scales which brought Noble prize to the developers Gerd Binnig and Heinrich Rohrer [44]. This technique depends on feedback loop which regulates the distance between the probe and the surface. This technique has paved the way for developments of other microscopy techniques as well using similar feedback control systems.

Scanning Tunnelling Microscopy relies on quantum tunnelling phenomena. It is suitable for conducting and semiconducting surface investigations at nanoscopic scales. Tunnelling phenomena depends on the possibility of an electron in motion passing through an energy barrier with higher energy level than the particle has. The expression of this motion has been presented by Schrödinger [45]. This principle was used in STM by applying potential difference between tip and sample as represented in Figure 2.3. The function in terms of tunnelling current and bias voltage that the STM operation relies on is given by formula 2.3 [46].

$$\mathrm{I_{tunnel}(z)} \approx \sum_{Ef-V}^{E_F} |\Psi(0)|^2 \mathrm{e}^{-1.025\sqrt{\varphi}\mathrm{z}} \approx V\rho_s\left(0, E_f\right) e^{-1.025\sqrt{\phi}z} \tag{2.3}$$

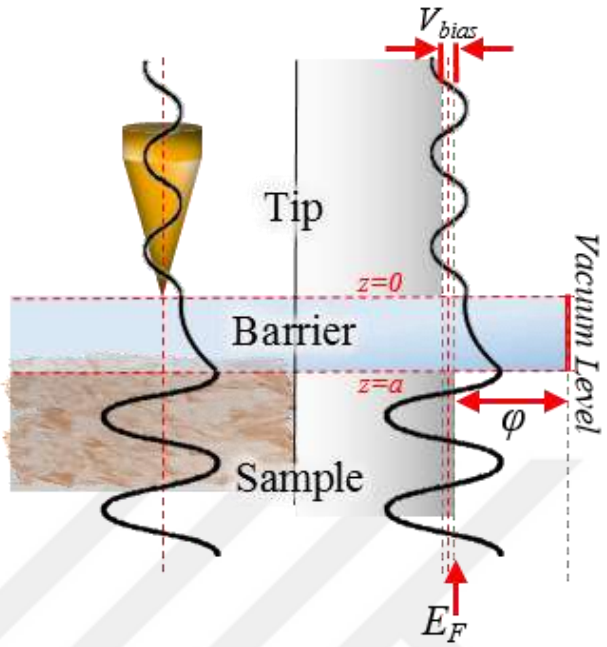

Figure 2.3 : Representation of quantum tunnelling phenomena of STM junction The gap with distance *a* yields potential region.

Feedback control system receives real-time responses from tunnelling current which allows electron density of state mapping during a scan [46, 47]. Based on the relation 2.3, two modes of STM operation have been in use; constant height mode and constant current mode.

In constant height mode, piezoelectric material does not move the tip on z-axis. Because of the morphology, tip-surface distance consistently changes during a linear scan. Based on formula 2.3, changes in *z* parameter yields differences in tunnel current which are mapped pixel by pixel. However, tip-crash is always possible for rough surfaces. Another mode is constant current mode that tunnelling current is set to a constant value. The tip is retracted/approached from/to the surface by the control system when the tunnel current tends to change depending on changes in the tip-surface distance due to the morphology. Tip moves by piezoelectric on z-axis during a linear scan is mapped pixel by pixel which gives topography of even rough surfaces. In this work, surface characterisations using STM were performed using constant current mode.

2.2.3 Photon mapping using scanning tunnelling microscope

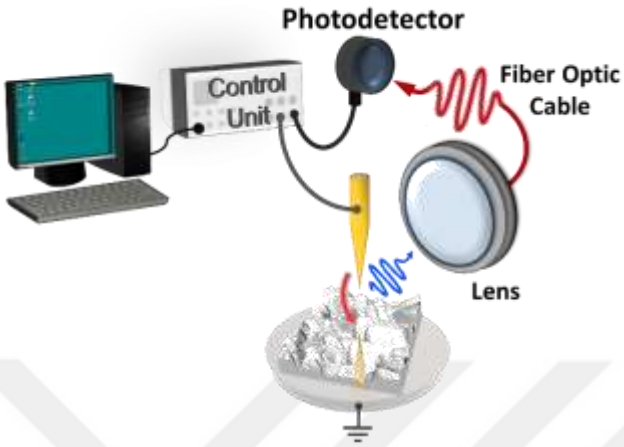

Figure 2.4 : Schematic diagram of Photon Emission Scanning Tunnelling Microscopy (pSTM) showing combination of photon collection components and STM.

Using a combination of optical components and a commercial STM device, it is possible to observe photon radiation characteristics of various surfaces. As shown in Figure 2.4, emitted photons are collected by a lens system and fibre optic cable, then converted to voltage signal by a photodetector. Control unit matches received data from STM piezoelectric material and photodetector, it presents simultaneously taken photon emission map of an STM image.

Table 2.1 : Electromagnetic spectrum wavelength ranges of different materials.

Material	Electromagnetic Spectrum Wavelength Range (nm)
Silicon	190-1100
Germanium	400-1700
Indium gallium arsenide	800-2600
Lead (II) sulphide	1000-3500
Mercury cadmium telluride	4000-14000

Semiconductors are used in photodetector devices preferably with PIN structures. Band gap of PIN structure varies depending on the material. As a result of it, material choice is decisive considering desired range of the investigation as shown in Table 2.1.

2.2.4 Atomic force microscope

Scanning Tunnelling Microscopy has opened a new area for atomic scale studies, however scope of specimen variety was limited with only conductive ones. Because of tunnelling current occurs only between conducting or semiconducting sample surface and STM tip, other materials were excluded from atomic scale investigations. Based on the idea that imaging of insulator surfaces as well, a new microscopy technique was developed which relies on measuring interatomic force between the probe and the surface [48].

$$V_{LJ} = \frac{a}{r^{12}} + \frac{c}{r^{6}} \tag{2.4}$$

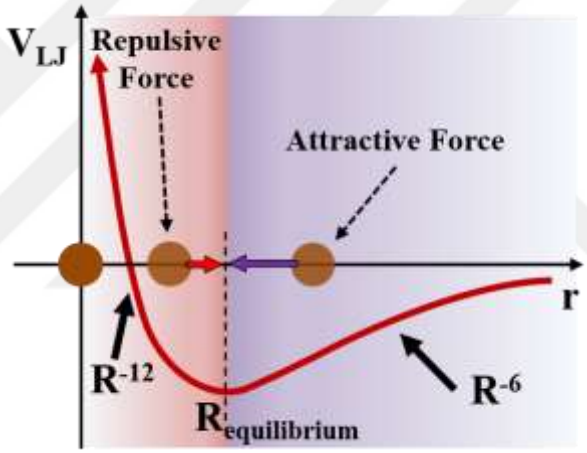

Figure 2.5 : Lennard-Jones potential with possible interatomic interactions based on the distance between two neutral atoms.

Interaction force between a pair of neutral atom or molecule was defined as *Lennard-Jones Potential* [49, 50]. Charge characteristics of these atoms or molecules shows attractive and repulsive force characteristics based on the distance between them (Figure 2.5). If the distance *r* is small enough, charge clouds overlaps and repulsive force becomes dominant due to Pauli principle. If *r* is bigger than equilibrium distance, attractive force appears as a result of dipole-dipole attraction.

As illustrated in Figure 2.6, a tip is attached to a cantilever which is regulated by driving piezoelectric. Based on equation 2.4, the tip is approached to the surface until cantilever is tend to bend by interatomic forces. Constants *a* and *c* are empirical values of the equation. Not only bending force is measured, but also deflection sensor is recorded as

feedback response. A laser beam is incident onto the cantilever where the tip is attached to the back side. Incident laser beams are reflected onto a quadrupole diode sensor. Signal differences between these four sensor segments are measured as deflection which is compared with initial values. Using this method, AFM can be operated with both static and dynamic modes.

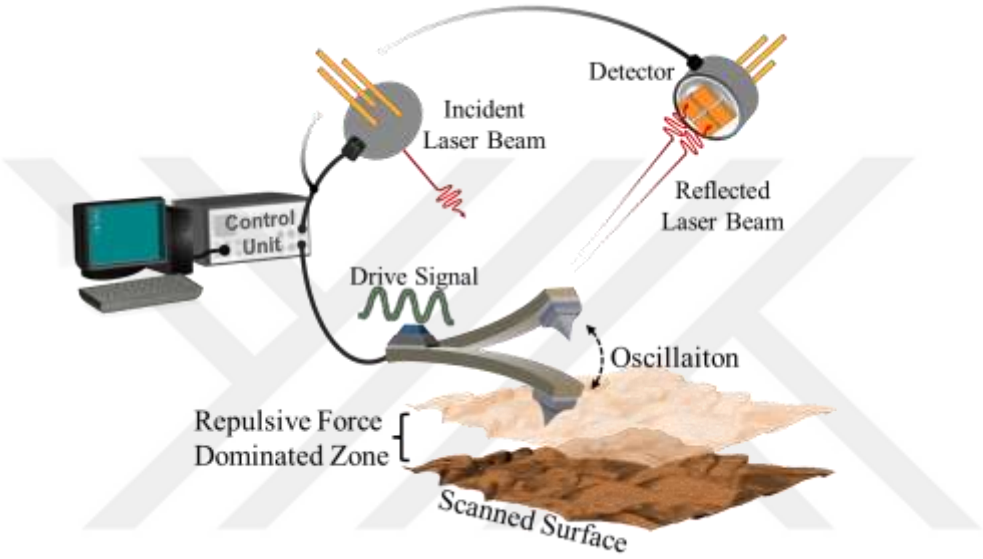

Figure 2.6 : Schematic diagram of Atomic Force Microscopy (AFM) operated with dynamic mode.

In this study, dynamic mode has been used due to low damage risk for rough surfaces as well. Piezoelectric material drives signal and oscillates cantilever near resonance frequency. This oscillation was modelled based on damped harmonic oscillator. Deflection signals of the oscillation are measured in terms of amplitude (A), frequency (*f*) and phase (φ). According to the needs of the investigation, amplitude or frequency can be set to a constant value as feedback parameter. During a scan, surface forces originated from the surface characteristics changes oscillation until feedback system regulates. Measurement changes in terms of these variables are mapped line by line which provides AFM images.

3. EXPERIMENT

3.1 Samples

3.1.1 Au/Mica and Au/Cr/Mica

Au samples were prepared with thermal evaporation, at 10^{-6} Torr pressure with 0,1-0,2 Å/s deposition rate. Thickness of Au film on Mica was 150 nm. Au/Mica sample has been studied for over a year so it has been exposed to air for a relatively long time. For Au/Cr/Mica, Cr layer has a thickness of 10 nm beneath Au film with 142 nm thickness. It was freshly prepared and inspections have started right after preparation.

3.1.2 Graphene on copper

Figure.3.1 : Split oven (left) and tube oven (right) setups which have been used for CVD grown graphene production [51].

Graphene on Cu samples were prepared by using a home built atmospheric pressure chemical vapour deposition (AP-CVD) system. 25 μm thick Cu foils (Goodfellow CU000420 with 99.95% purity) were first cut to sizes of 5 mm x 5 mm, and rinsed in IPA. Following that, copper foil pieces were placed on a quartz plate (Schott) and located at the centre of a quartz tube (Schott) inside a temperature controlled tube oven. After the foil pieces were placed in the oven, a mixture of Ar (%99.995 pure, Linde) and H2 (%99.99

pure, Linde) was let in to the tube with flow rates of 1000 sccm for both and samples were heated up to 1000 °C with a heating rate of 7°C/min. Flow rates were controlled by Dwyer RM-series manual flow meters. In order to prevent any atmospheric backflow in to the quartz tube and stabilize the pressure, a bubbler was placed at the exit port of the tube. After the system has reached to the annealing temperature, samples were kept at around 1000 °C for 30 min. Then, the flow rate of hydrogen was decreased to 60 sccm and CH_4 (%99 pure, Linde) was let into the tube with a flow rate of 10 sccm for 5 minutes for graphene formation. After exposure to CH_4 samples were cooled under Ar-H_2 flow atmosphere with 12^{o}C/min cooling rate and they were taken out of the tube oven.

3.1.2 Graphene transferred samples

Due to graphene growth is possible using methods that are limited by the number of substrate variety, graphene layer has been transferred onto different substrates. Polymethyl-methacrylate (PMMA) mediated process has been followed in this work [38]. The process includes coating graphene/Cu sample with PMMA, removing copper with etching by $FeCl_3$ solution, than dissolving PMMA after graphene is transferred on the new substrate.

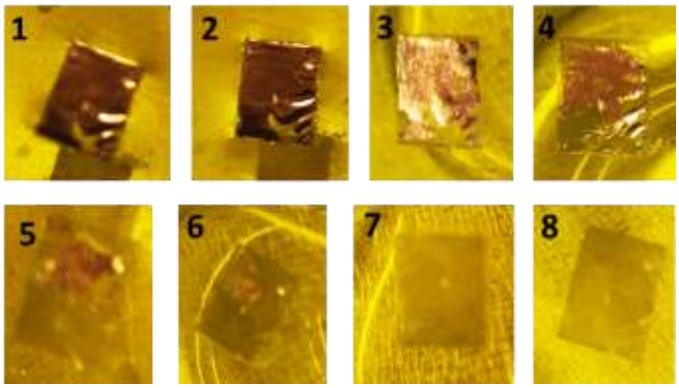

Figure 3.2 : Dissolving process of copper beneath graphene in $FeCl_3$ solution.

PMMA (5 mg/ml) was dissolved in acetone at room temperature. That prepared solution was dropped onto Graphene/Cu sample which was mounted on spin-coater (1000 rpm for 30 seconds). As shown in Figure 3.2, copper substrate was etched from PMMA covered graphene in $FeCl_3$ (0.4 mole/l) solution. When copper is completely dissolved (Figure 3.2) was started being diluted using de-ionised water (DI-water). Free standing

Graphene+PMMA was picked up using new substrates such as SiO_2, Si and Au. For the vaporisation of intercalated water left from the process, PMMA/G/Substrate sample was left in a desiccator for 12 hours. The last step was dropping sample in acetone to get rid of PMMA.

3.2 Atomic Force Microscope

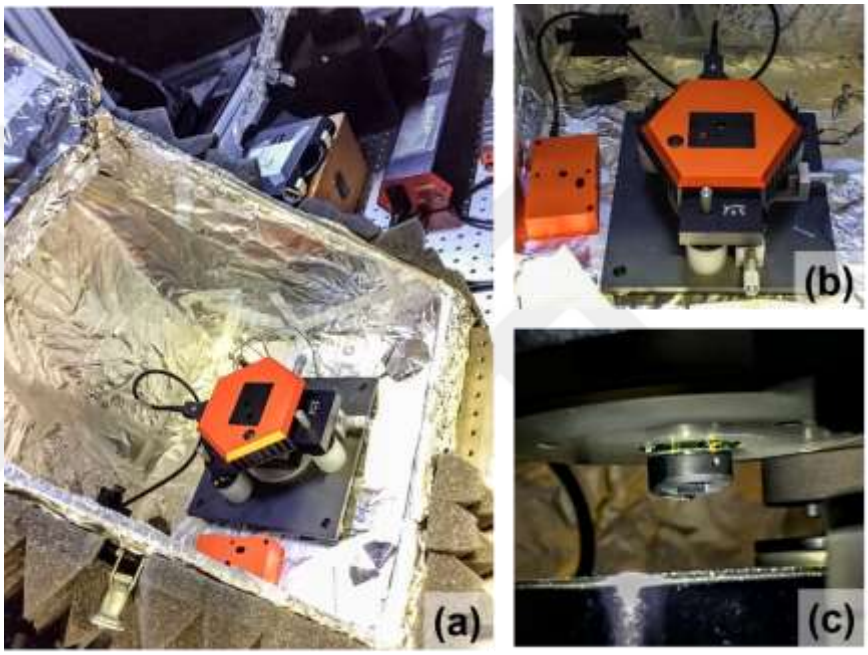

Figure 3.3 : Nanosurf™ Flex-AFM mounted on a floating optical table which was isolated from external vibrational and light noise.

A commercial Nanosurf™ Flex-AFM was used for the surface investigations before photon STM studies. Measurements have been operated in dynamic mode. NANOSENSORS™ PPP-NCHR probe was attached to the cantilever which as tip apex smaller than 7 nm and 10-15 μm tip height.

3.3 Photon Scanning Tunnelling Microscope

In this study, photon emission experiments were performed with tip-biased Nanosurf™ Easyscan 2 STM head under ambient conditions in a floating dark box using constant current mode. Optical photon collection set up was assembled in the laboratory [52].

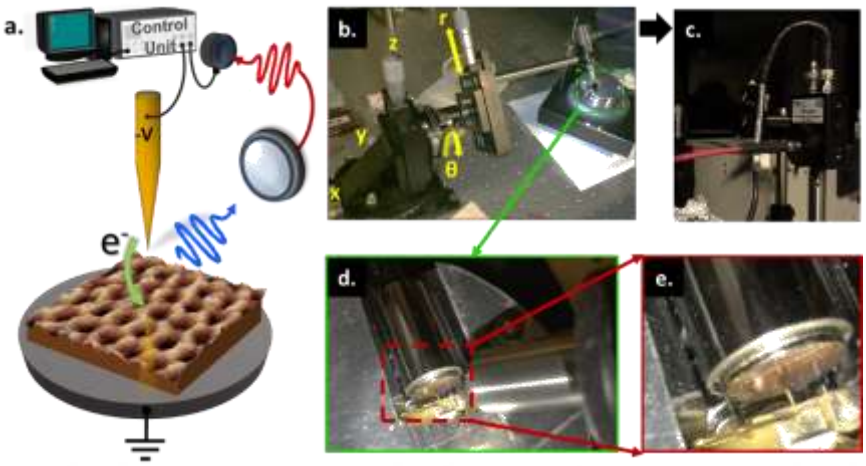

Figure 3.4 : Photon Emission Scanning Tunnelling Microscope (pSTM) Setup which was assembled with optical collection setup in the laboratory. The setup mounted on a floating optical table which was isolated from external vibrational and light noise.

Photon collection mechanism on STM head was designed and assembled by using commercially available stages and optical components providing five degrees of freedom (Figure 3.4). Several studies have already shown that positioning of optical components is crucial for the observation of different modes of angle-dependent photon emission. The setup was mounted on a floating optical table which was isolated from external vibrational and light noise. Emitted photons from tunnelling junction were collected with an aspheric lens (A397TM -B), mounted on collimation package (THORLABS® F280SMA-A) and protected silver reflective collimator (THORLABS® RC04SMA-P01) which was connected to a fibre optic cable (THORLABS® M30L01) which transfers collected photons to the femtowatt photo receiver (THORLABS® PDF10A/M) from the STM tunnel junction. The output of the photo receiver was connected to the STM control electronics as an additional surface mapping channel. Photon emission data were taken simultaneously with the STM topography data for every scan pixel. This gave the opportunity to make real-time photon emission mapping of the surface with the STM topography and tunnelling current maps of the surfaces.

In addition, output signal of the photodiode which is in volts was converted to power in femtowatt, to better interpret taken photon maps. Following formula 2.5 was used;

$$V_{out} = P_{opt} \times R(\lambda) \times G \qquad (2.5)$$

where *G* represents the transimpedance gain (1 x 10^{12} V/A) of photodiode at room temperature. *R(λ)* is the function that is wavelength dependency of photodiode's responses to received photons. Noise of photodiode was measured as 0.05 V which was subtracted during analysis processes. Responsivity (A/W) versus wavelength profile was released by the manufacturer or photodiode as given in Figure 3.5 [53].

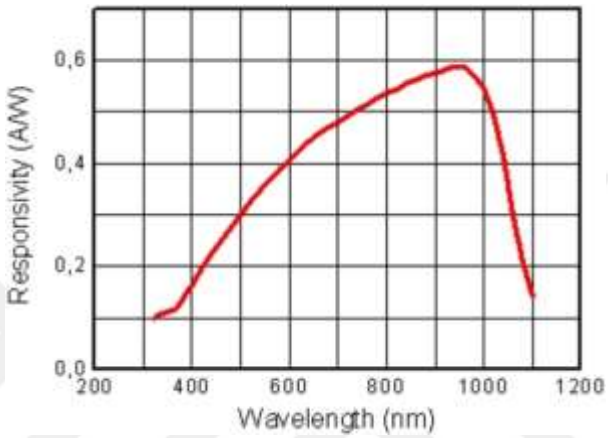

Figure 3.5 : Responsivity curve of THORLABS® PDF10A/M detector [53].

4. RESULTS AND DISCUSSION

4.1 Surface Characterisation of Graphene

Surface characteristics of graphene on copper which was produced in our laboratory has been investigated using Raman Spectroscopy, ambient AFM and STM respectively. All the results were compared with the reports on graphene properties in the literature.

Raman spectroscopy is a precise and non-destructive method identifying number of graphene layers. Terminology for interpretation of the spectral results has been named as *G* peak at 1582 cm^{-1} indicating graphene, *G'* peak at 2700 cm^{-1} indicating graphitic material, *D* peak at 1350 cm^{-1} indicating disordered characteristics of the investigated area [54, 55].

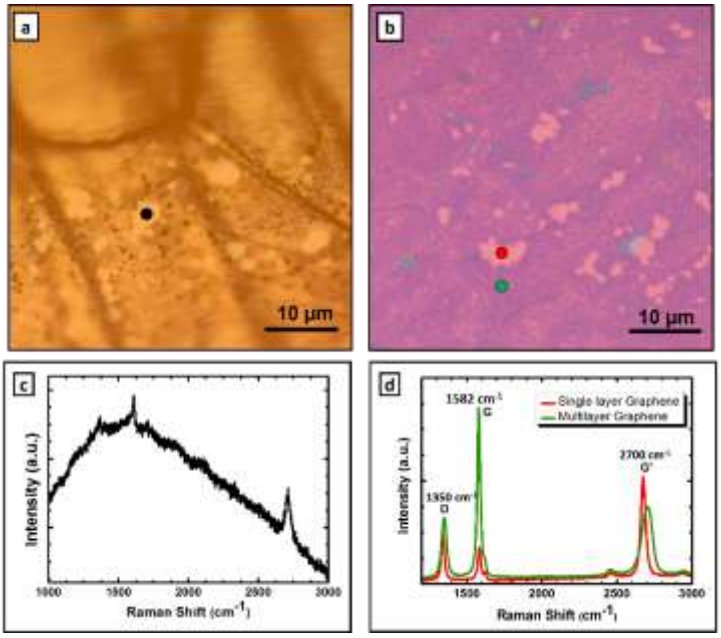

Figure 4.1 : Optical images of (a) graphene on copper and (b) transferred graphene on SiO_2 wafer. (c) Raman spectrum of single layer graphene on copper. (d) Raman spectra of single and multilayer graphene on SiO_2 wafer [51].

As shown in Figure 4.1, peaks fell on Raman shift values of single layer of graphene. Laser indicated zone on the single-layer graphene areas are discernible by being lighter coloured than multi-layer graphene zones. However, it is not easy to interpret intensity ratio of *G'* and *G* peaks (I'_G/I_G) due to curve characteristics yielded by fluorescence effect of copper substrate. To avoid this noise, graphene was transferred onto SiO_2 wafer and Raman spectroscopy was performed over G/SiO_2 surface. Red spot shown in Figure 4.1(b) indicated single layer of graphene with the intensity ratiou of *G* and *G'* peaks. On the other hand, green spot shown in Figure 4.1(b) again yielded higher *G* peak than *G'* which means investigated area has multilayer graphene structure.

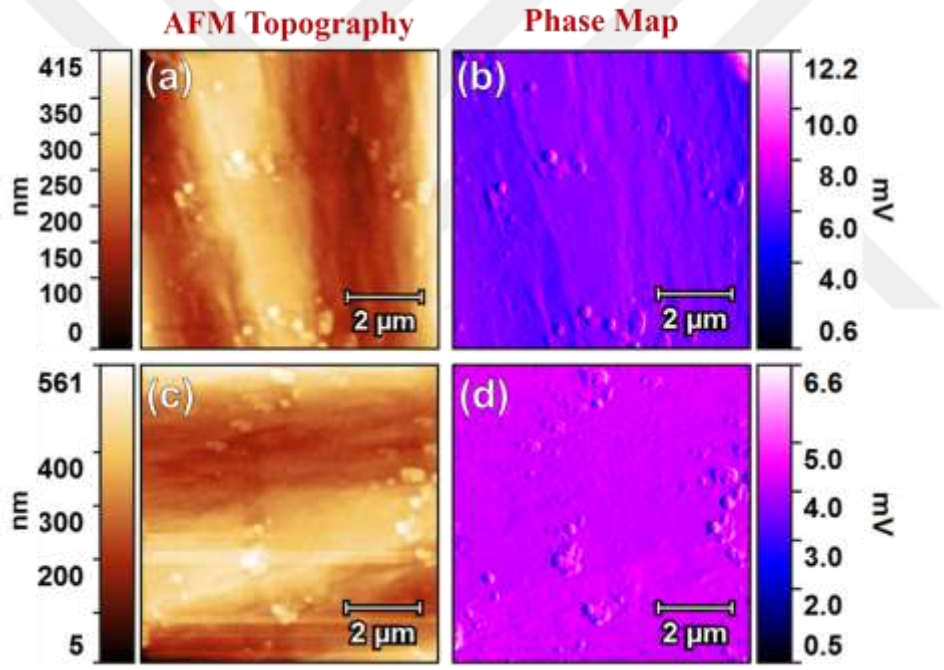

Figure 4.2 : (a, c) Topographies and (b, d) phase maps of G/Cu mounted AFM surface investigations..

Graphene on copper surfaces were mounted on AFM for large area topography investigations under ambient conditions, after Raman spectroscopy analysis. As given in Figure 4.3, surface roughness was dominated by Copper substrate beneath graphene and impurities. On the other hand, impurities on the surface have a negative effect on the scan stability. Based on these measurements, STM scans on smaller areas were expected to have smoother characteristics with the possible observation of atomic terraces.

Clearly it is not possible to image Cu surfaces under ambient conditions due to their reactivity. Thus, a stable tunnelling with an STM tip on to pristine Cu surface is practically

impossible which means a proper imaging requires UHV conditions. However, protection by the grown graphene layer(s) enabled investigations of atomic step and terrace characteristics of copper substrate under ambient [56].

In this part, surface characteristics of graphene on copper which was produced in our laboratory has been investigated using ambient STM. Prior expectations from STM studies of graphene surface were observation of continuity over substrate facets, atomic resolution and different formations due to occurred stresses on the step edge, super-periodicity and abnormal nucleation [56, 57].

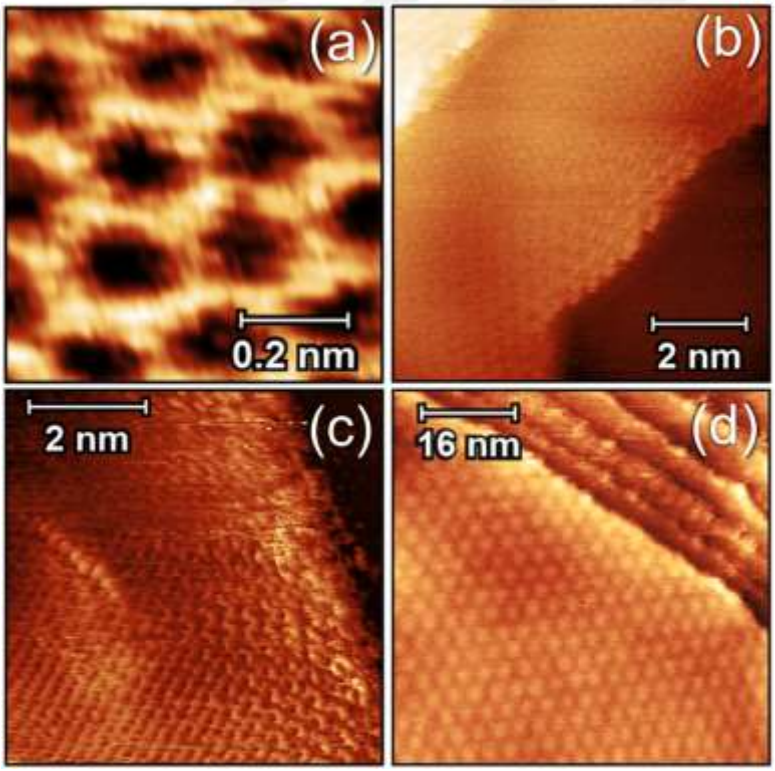

Figure 4.3 : Set parameters are It=450 pA and V_b=50mV for all STM images above. (a) Honeycomb atomic resolution from a small scan area, (b) partial moire seen in the middle terrace where continuous graphene layer over copper, (c) *croissant* like periodic patterns at the edge of a terrace and (d) Moiré patterns on a flat terrace.

As shown in Figure 4.3, various forms of graphene on copper sample were observed using an ambient STM. Figure 4.3 (a) of hexagonal structure of a single graphene layer was observed under ambient conditions as well. Measurement of atomic resolution show that theoretical and experimental results are matching as illustrated in Figure 4.4. Continuity of graphene layer like a sprawled sheet even over step edges can be seen in Figure 4.3 (b).

This property was also a proof of how graphene protects substrate against corrosion *e.g.* oxidisation. Because of possible stress or periodically stacked multilayer graphene over step etched yielded *croissant* like structure as shown in Figure 4.3 (c). One of the best examples of super-periodicity between graphene-graphene or graphene-copper substrate atoms appeared as Moiré patterns [58] as shown in Figure 4.3 (d).

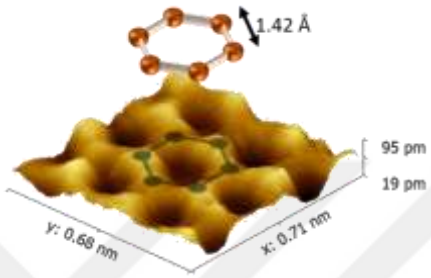

Figure 4.4 : Hexagonal structure of Graphene imaged with STM and its visual illustration.

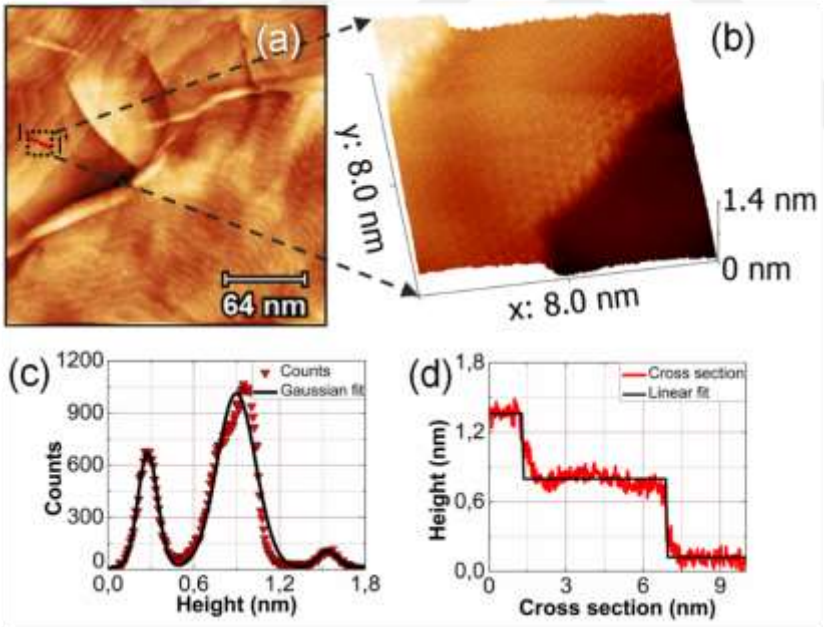

Figure 4.5 : (a) STM image of graphene on copper (It=450 pA and Vb=50mV). (b) Continuity of graphene over copper steps (It=0,3nA and Vb=0,05 V) is visible. (c) Height histogram and (d) cross section (I - I') analysis of copper steps.

Other benefit of continuous graphene is observation and analysis of substrate characteristics. Using this property, we measured step heights from our STM data, then compared with expected step height calculations for crystal identification (Figure 4.5). A single step height of Cu(111) facet is 0,208 nm, Cu(100) is 0,361 nm and Cu(110) is 0,255

nm respectively. As shown in Table 4.1, step height analysis of the chosen zone identified surface orientations of the terraces.

Table 4.1 : Step height analysis results of chosen zones shown in Figure 4.5. d_h and d_{cs} are measured step heights which were obtained by using histogram and cross section method respectively. d_{calc} is the expected distance between two copper planes. n is the number of layers between two corresponding copper planes. ε_h and ε_{cs} are error rates of histogram and cross section measurements.

	d_h (nm)	d_{cs} (nm)	d_{calc} (nm)	n	Facet	ε_h (%)	ε_{cs} (%)
Upper Step	0,641	0,578	0,627	3	Cu(111)	2,3	7,7
Lower Step	0,621	0,677	0,627	3	Cu(111)	0,9	7,9

Figure 4.6 presents a unique Moiré characteristics on a large scan area. Although graphene covers all the substrate surface, these super-periodic patterns appeared only over one direction. The reason was claimed to be super-periodicity between honeycomb graphene crystal and hexagonal Cu(111) facet which have low atomic mismatch.

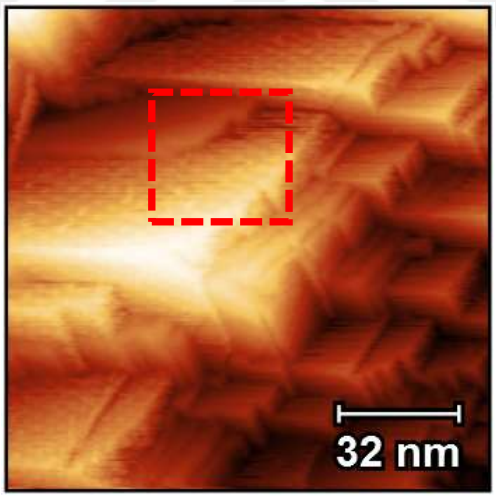

Figure 4.6 : STM images showing 128 nm x 128 nm (b) sample region of G/Cu with moiré patterns (Set parameters: It=450 pA and Vb=50mV).

Other analysis from the measurement given in Figure 4.6 was Moiré pattern investigation using different bias voltages. As Figure 4.6 (a to i) have revealed, Moiré patterns disappeared step by step as a result of electrons from different states were projected depending on the applied bias voltages. This case was also named as *tuneable transparency of graphene* by Herrero [59]. This claim has also been supporting the idea that electronic interaction between Cu(111) and graphene occurs only on the surface states.

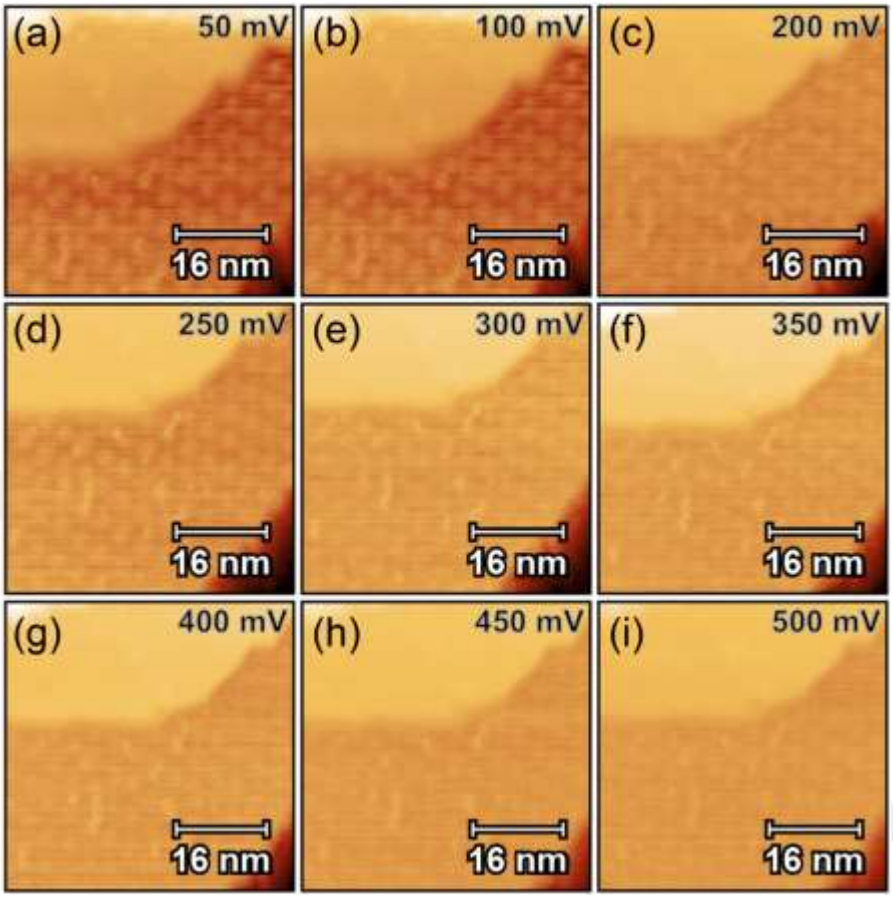

Figure 4.7 : STM images of a selected area shown with red dashed lines in Figure.3.2.1. Figures (a to i) show tuneable transparency of graphene, thus, Moiré patterns under different bias voltages (It=450 pA for all the measurements).

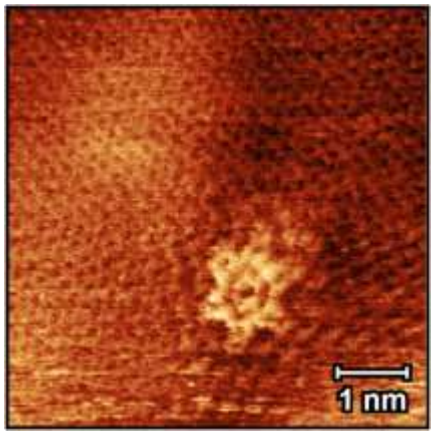

Figure 4.8 : STM images showing 8 x 8 nm2 sample region of G/Cu with *flower-like* formation of point defect. (Set parameters: It=450 pA and Vb=50mV).

Abnormal structures of carbon atoms *e.g flower defects* [57, 61] were also observed as shown in Figure 4.8. Even if graphene has strongly bonded hexagonal crystal structure, a mutant bonding may also occur with a missing or an extra atom.

To sum up, our surface characterisation of homemade graphene on copper sample which was grown with CVD has presented most of the cases in the literature. These results have proved reliability of the sample and the measurement setup. As shown above, step height and crystal orientations can be identified and reliable STM scans can be performed under ambient conditions.

4.2 Tunnelling Induced Photon Emission from STM Junction

4.2.1 Tip and emission calibration using Au/Mica and Au/Cr/Mica

Different tips were prepared to utilise photon emission investigations using scanning tunnelling microscope. Diameter of the wire was required to be 0,25 mm for the measurement device Nanosurf^{TM} Easyscan 2 STM. Electrochemically etched Au, mechanically cut $Pt_{80}Ir_{20}$, mechanically cut homemade $Au_{80}Ag_{20}$ tips were compared in terms of scan quality, endurance and emission.

Figure 4.9 shows photon emission scanning tunnelling microscopy (pSTM) calibration measurements using various tips and their scans on the right side each. Au was the softest and the most deformable one of all. Even though electrochemical process shaped the tip ideally, it has been inefficient due to being comparatively very long and troublesome than mechanical cut. $Pt_{80}Ir_{20}$ shaped by mechanical cut appeared as good option based on topography measurements. However, it was decided as ineffective due to spikes when high bias voltage was applied for pSTM investigations. Measurements taken by using homemade $Au_{80}Ag_{20}$ tips were surprisingly satisfying in terms of both STM topographies studies and photon emission maps. As a result, $Au_{80}Ag_{20}$ tips has been used for further investigations.

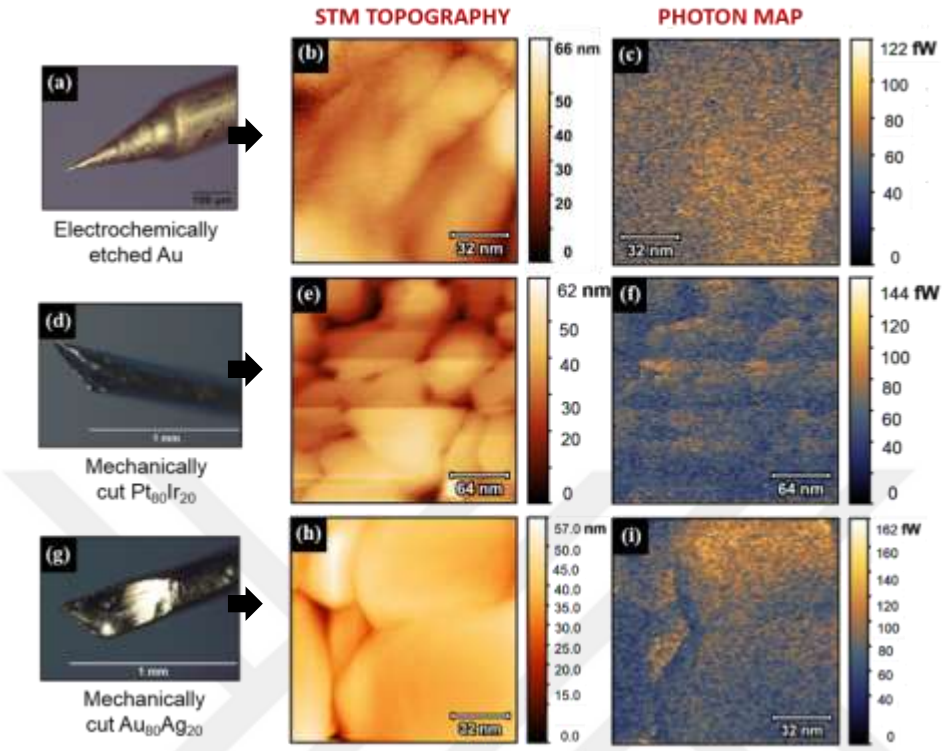

Figure 4.9 : (a, d, g) Different tips prepared using various materials and shaping methods were used in Au/Mica sample mounted pSTM investigations. Tunnelling parameters were (b, c) I_t= 22 nA and V_{bias}=-1.8 V, (e, f) I_t= 30 nA and V_{bias}=-1.8 V, (h, i)) I_t= 22 nA and V_{bias}=-1.7 V respectively.

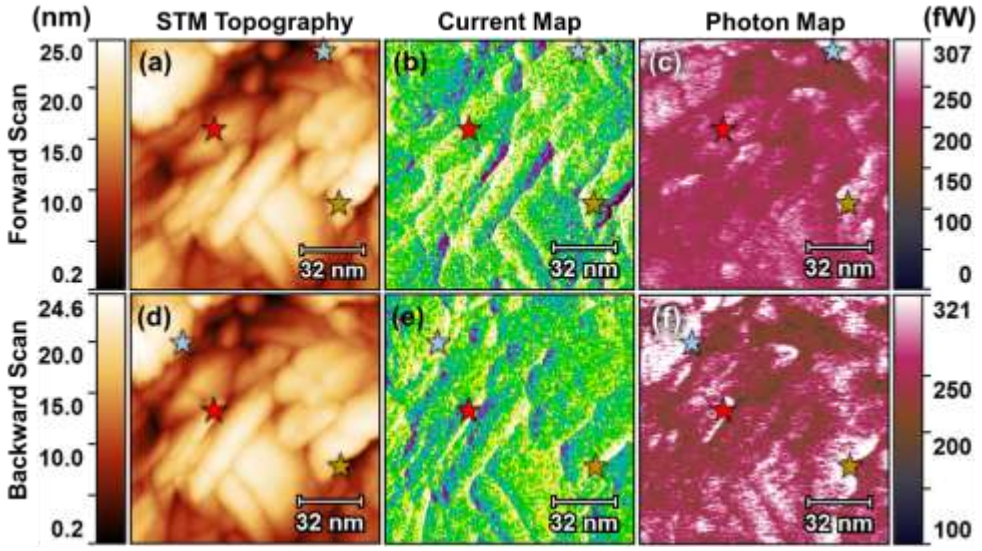

Figure 4.10 : Simultaneously taken STM topography, current map and photon map of (a, b, c) forward and (d, e, f) backward scans of Au/Cr/Mica mounted pSTM investigations. Tunnelling parameters were I_t= 25 nA and V_{bias}=-1.5 V.

After $Au_{80}Ag_{20}$ was chosen as the tip material of pSTM investigations, possible parameters that photon emission may base on were investigated. Au/Cr/Mica sample was mounted. In Figure 4.10, coloured stars were used to track chosen points between STM topography, current map and photon map. Results have revealed that photon emission relies on how the tip approaches to a grain. For instance, PE was observed on the left side of the grains during forward scans and on the right side of the same grains for backward scans (Figure 4.10). This indicates that the occurrence of photon emission can be originated to localised surface plasmon (LSP). Intensities were maximum at the step edges and attenuated along the grain on the scan direction. In this case, current map also showed relation between intensity of photon emission and scan direction. Maximum intensity and current values corresponded to where the tip was extremely close to the surface for a moment until retracted by feedback.

4.2.2 Graphene on copper

In this section, photon emission observation from the tunnel junction between the STM tip and graphene on copper surface under ambient conditions was presented. Photon emission maps and simultaneously taken STM topographies showed an obvious correlation. However, it was different than photon emission studies with calibration specimens. Unlikely to the photon maps taken Au/Mica and Au/Cr/Mica surfaces, photon emission appeared as spreading through wider areas on the surface having similar intensity. Moreover, photon emission characteristics of G/Cu did not change for forward and backward scans in contrast to calibration samples. In further steps, analysis of photon emission properties were presented in terms of intensity and topography correlation.

Tunnelling current induced photon emission maps of the graphene/Cu samples have presented wide emissive or non-emissive zones. Photon maps were not depending on only to the grains of the noble metal substrate. Such data (Figure 4.12 and 4.13) clearly brought many questions with them. First of all, the reason of the emitted photons form this system needs to be understood.

We will discuss the possible origins of the photon emission by considering both single layer and multilayer graphene existence on the investigation area. The variation of the photon emission from the G/Cu surface position to position even on the same scan system

can be due to some reasons such as: Photons were generated by the occurrence of the free electron like surface states forming between G/Cu may lead to the generation of gap plasmons at the tunnel junction and decays into surface plasmon polaritons along the surface under special conditions [6].

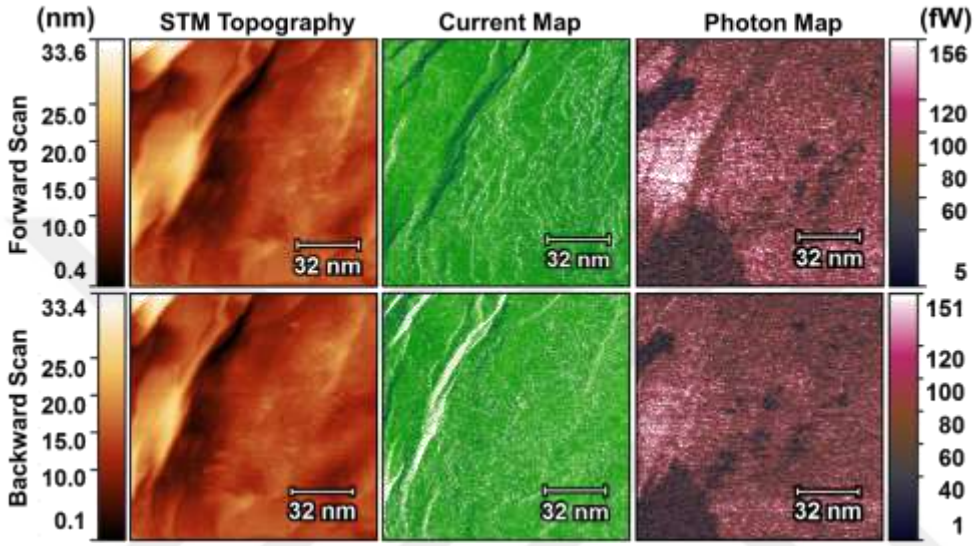

Figure 4.11 : Simultaneously taken STM topography, current map and photon map of (a, b, c) forward and (d, e, f) backward scans of G/Cu mounted pSTM investigations. Tunnelling parameters were I_t= 21 nA and V_{bias}=-1.8 V.

In contrast to Au/Cr/Mica as given in Figure 4.10, results of G/Cu sample have revealed that photon emission does not on how the tip approaches to a grain (Figure 4.11). For instance, PE was observed homogenously over wider zones. Moreover, PE did not change for forward and backward scans. On the other hand, there is no correlation with photon map and current map in this system. This indicates that the occurrence of photon emission might depend on different mechanisms different than LSP originated photon emission from Au/Cr/Mica. In order to study the dependency of the photon emission to the Cu facets, high resolution scans were taken from photon emissive and non-emissive zones. As it can be seen in Figure 4.12, three analysis zones were chosen from emissive zones. This measurement showed a homogeneous emissivity except for surface impurities. Darker areas on the photon map corresponding to impurities of the surface which are also non-emissive. Step height measurements using cross-section and colour histogram analysis method (Figure 4.13) defined their crystal orientations of chosen emissive areas.

As shown by Table 4.2, both analysis methods determined that these three zones are Cu(111).

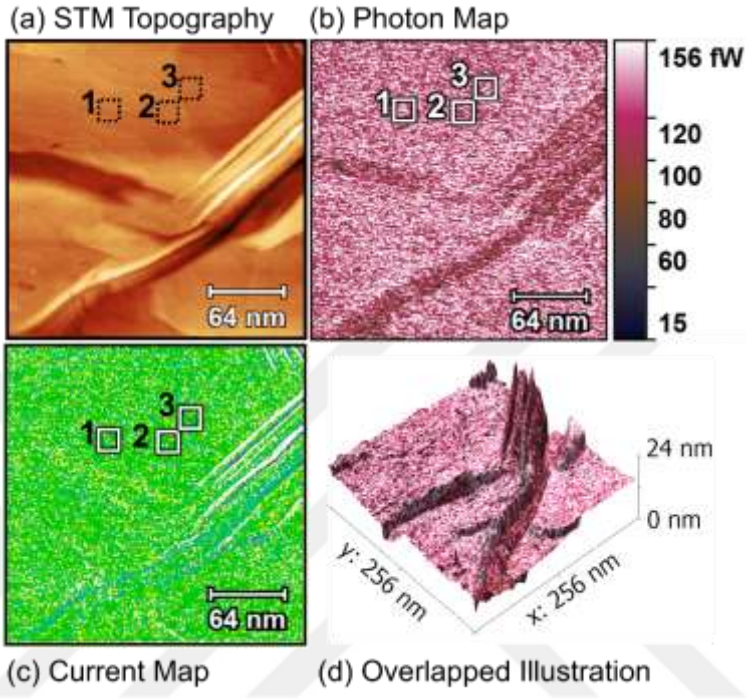

Figure 4.12 : (a) STM image, (b) photon map, (c) current map and (d) overlapped photon map on 3D illustration of topography showing 256 nm x 256 nm sample region of G/Cu (Set parameters: It=40 nA and Vb= -2.1V). Zones numbered as 1 to 3 were analysed in terms of Miller indices and photon emissivity.

Similarly, three analysis zones were chosen from another measurement as it can be seen in Figure 4.13. This scan also showed homogeneous emissivity except for surface impurities. As given in Figure 4.14, bright areas on the photon map are corresponding to wide polycrystalline copper grains underneath graphene while darker areas are corresponding to impurities again. Step height measurements using cross-section and colour histogram analysis method (Figure 4.15) identified their crystal orientations of chosen emissive areas. As shown by Table 4.3, both analysis methods showed that these three zones are are corresponding to Cu(111) underneath graphene layer.

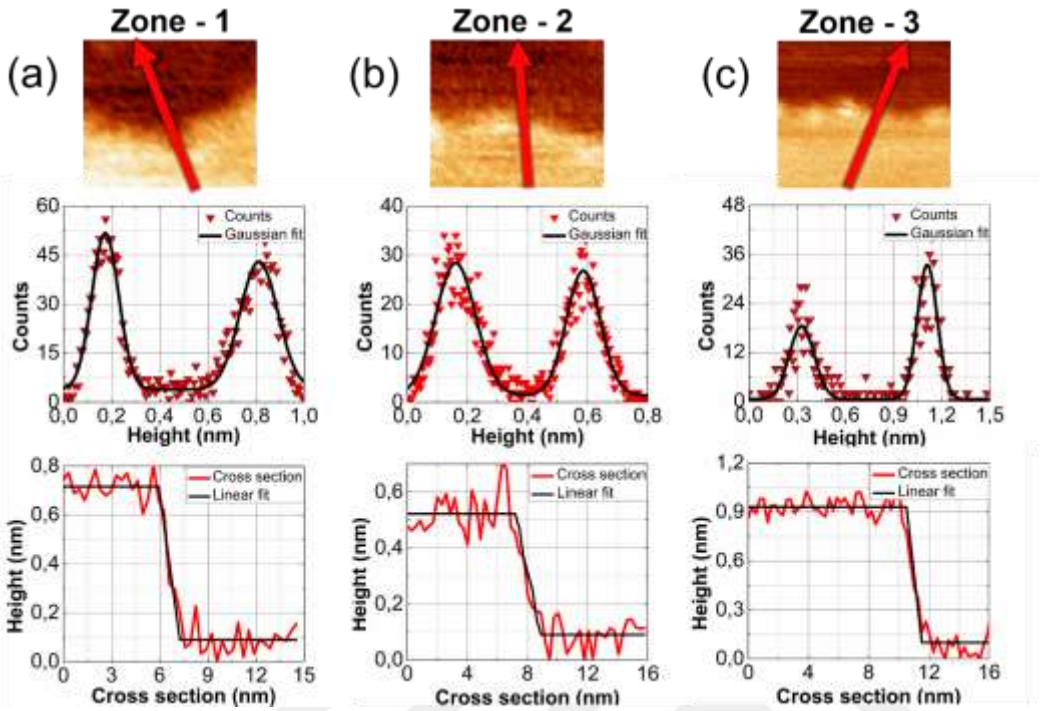

Figure 4.13 : Chosen zones from Figure 4.12 STM topography image in the first row. Graphs on the second row are histogram and the third row are line-scan analysis results.

Table 4.2 : Step height analysis results of chosen zones as it is shown in Figure 4.13. d_h and d_{cs} are measured step heights which were obtained by using histogram and cross section method respectively. d_{calc} is the expected distance between two copper planes. n is the number of layers between two corresponding copper planes. ε_h and ε_{cs} are error rates of histogram and cross section measurements. Photon emission (PE) observations were also given in the rightmost column.

Zone	d_h (nm)	d_{cs} (nm)	d_{calc} (nm)	n	Facet	ε_h (%)	ε_{cs} (%)	PE
1	0,631	0,628	0,628	3	Cu(111)	0,6	0,004	Yes
2	0,425	0,418	0,418	2	Cu(111)	1,6	3,4	Yes
3	0,789	0,831	0,836	4	Cu(111)	5,6	0,6	Yes

An additional cross-section analysis was done to understand profile of the impurity shown as the arrow from I to I' in Figure 4.14(a). Line profiles taken by applying 50 mV and 2.1 V given in Figure 4.16 indicates that the scan area might have multilayer graphene structure. As Lalmi has already reported [59], these wrinkles may occur as a result of multilayer graphene formation. Due to applied high bias voltages, graphene layers staying beneath may rise towards to the topmost layer. This may appear as variance in electronic characteristics yielding line profiles with different heights as given in Figure 4.16.

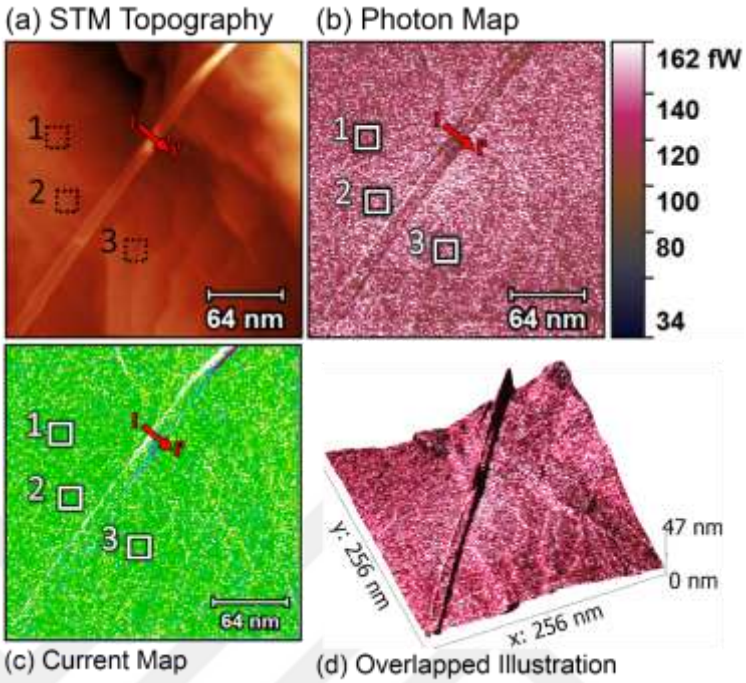

Figure 4.14 : (a) STM image, (b) photon map, (c) current map and (d) overlapped photon map on 3D illustration of topography showing 256 nm x 256 nm sample region of G/Cu (Set parameters: It=40 nA and Vb= -2.1V). Zones numbered as 1 to 3 were analysed in terms of Miller indices and photon emissivity. I-I' indicates where the cross section was taken.

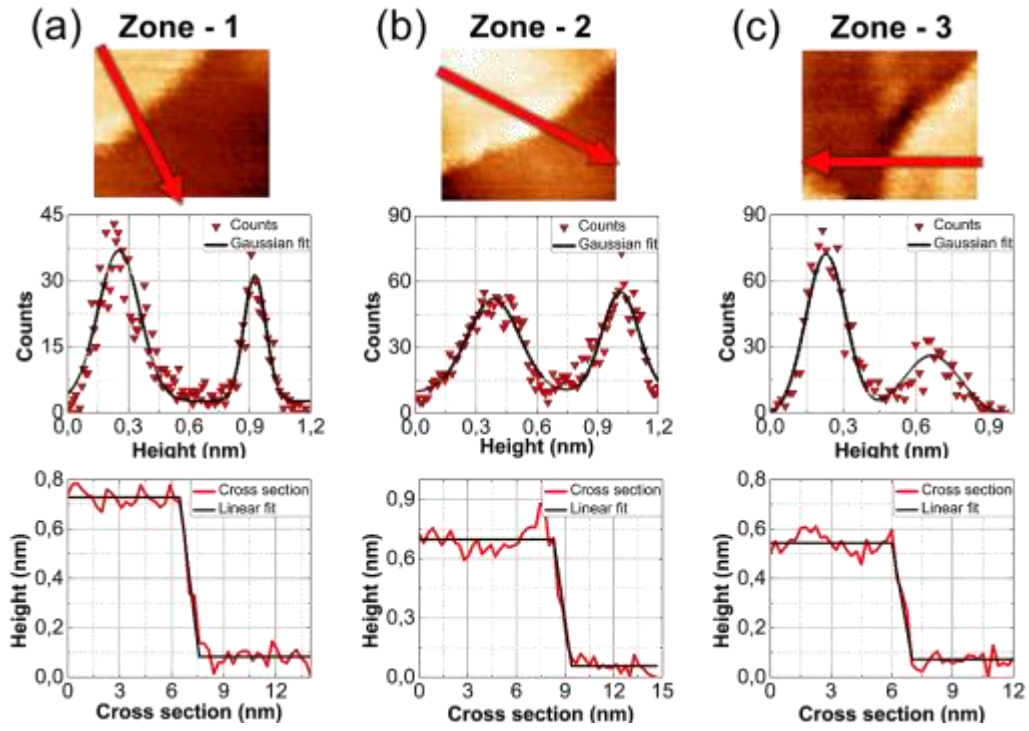

Figure 4.15 : Chosen zones from Figure 4.14 STM topography image in the first row. Graphs on the second row are histogram and the third row are line-scan analysis results.

Table 4.3 : Step height analysis results of chosen zones as it is shown in Figure 4.15. d_h and d_{cs} are measured step heights which were obtained by using histogram and cross section method respectively. d_{calc} is the expected distance between two copper planes. n is the number of layers between two corresponding copper planes. ε_h and ε_{cs} are error rates of histogram and cross section measurements.. Photon emission (PE) observations were also given in the rightmost column.

Zone	d_h (nm)	d_{cs} (nm)	d_{calc} (nm)	n	Facet	ε_h (%)	ε_{cs} (%)	PE
1	0,658	0,644	0,627	3	Cu(111)	4,9	2,8	Yes
2	0,629	0,640	0,627	3	Cu(111)	0,4	2,1	Yes
3	0,429	0,456	0,418	2	Cu(111)	2,7	9,2	Yes

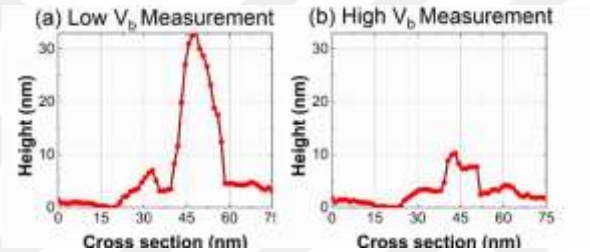

Figure 4.16 : Line-scan profile indicated by the arrow *I–I'* as shown in STM image Figure 4.14(a). Line profiles taken by applying (a)50 mV and (b)2.1 V.

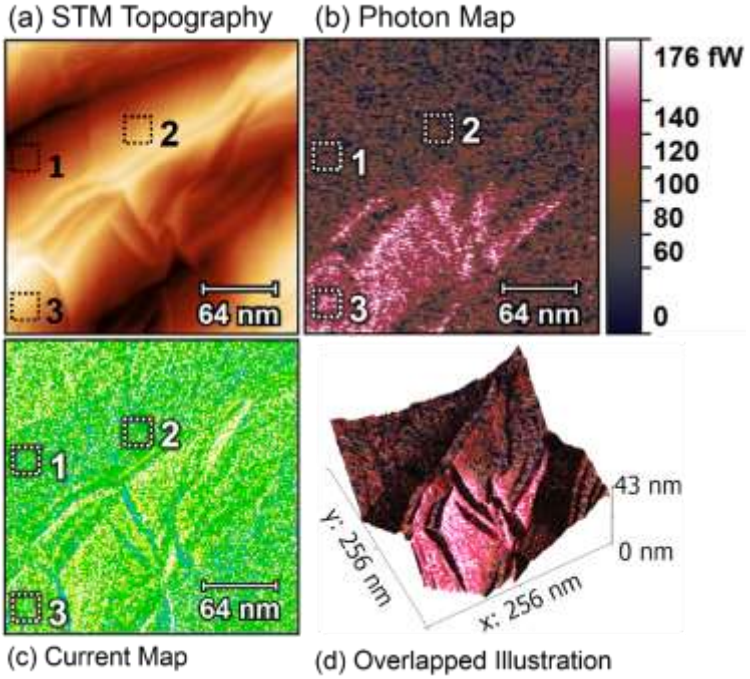

Figure 4.17 : (a) STM image, (b) photon map, (c) current map and (d) overlapped photon map on 3D illustration of topography showing 256 nm x 256 nm sample region of G/Cu (Set parameters: It=22 nA and Vb= -2.3 V). Zones numbered as 1 to 3 were analysed in terms of Miller indices and photon emissivity.

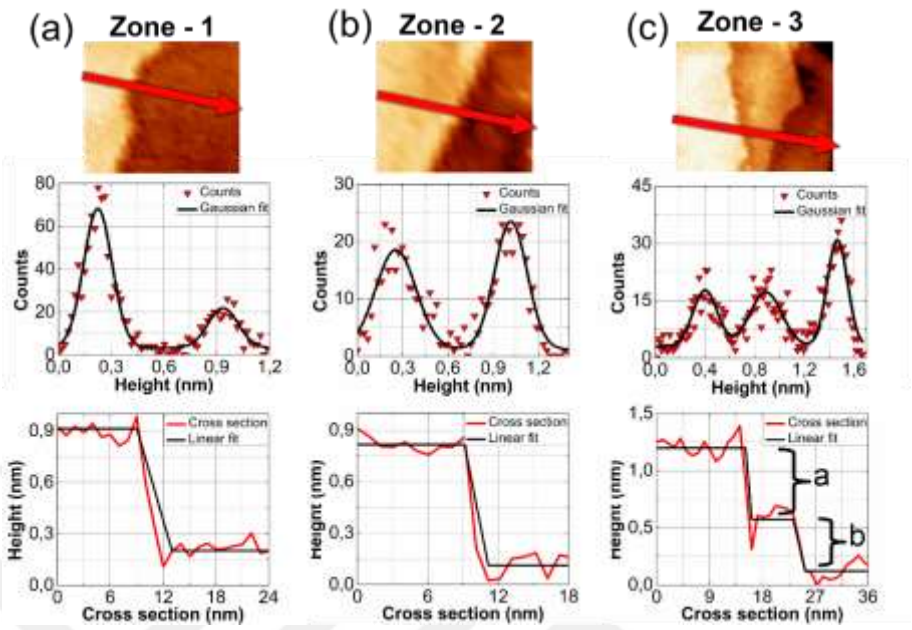

Figure 4.18 : Chosen zones from Figure 4.17 STM topography image in the first row. Graphs on the second row are histogram and the third row are line-scan analysis results.

Three analysis zones were analysed from another measurement as it can be seen in Figure 4.17. In this case, photon emission was seen particularly. According to the same steps of facet identification analysis, zone-1 and zone-2 correspond to Cu(100) faces where no photon emission was observed. On the other hand, both steps of zone-3 appeared as Cu(111) oriented facet where photon signals were received by photodetector.

Table 4.4 : Step height analysis results of chosen zones as it is shown in Figure 4.18. d_h and d_{cs} are measured step heights which were obtained by using histogram and cross section method respectively. d_{calc} is the expected distance between two copper planes. n is the number of layers between two corresponding copper planes. ε_h and ε_{cs} are error rates of histogram and cross section measurements.. Photon emission (PE) observations were also given in the rightmost column.

Zone	d_h (nm)	d_{cs} (nm)	d_{calc} (nm)	n	Facet	ε_h (%)	ε_{cs} (%)	PE
1	0,716	0,711	0,724	2	Cu(100)	1,2	1,8	No
2	0,732	0,704	0,724	2	Cu(100)	1,6	3,4	No
3.a	0,605	0,625	0,627	3	Cu(111)	0,3	3,6	Yes
3.b	0,447	0,452	0,418	2	Cu(111)	8,1	6,9	Yes

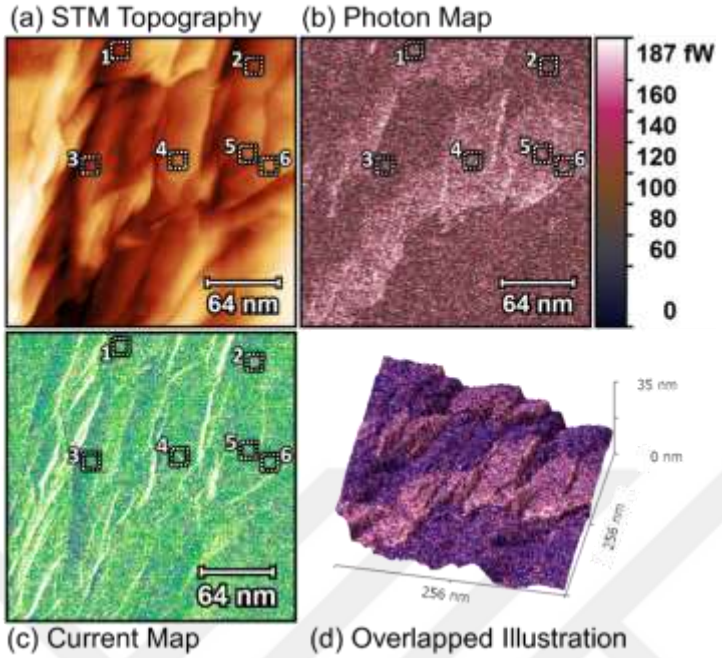

Figure 4.19 : (a) STM image, (b) photon map, (c) current map and (d) overlapped photon map on 3D illustration of topography showing 256 nm x 256 nm sample region of G/Cu (Set parameters: It=33 nA and Vb= -2.1V). Zones numbered as 1 to 6 were analysed in terms of Miller indices and photon emissivity.

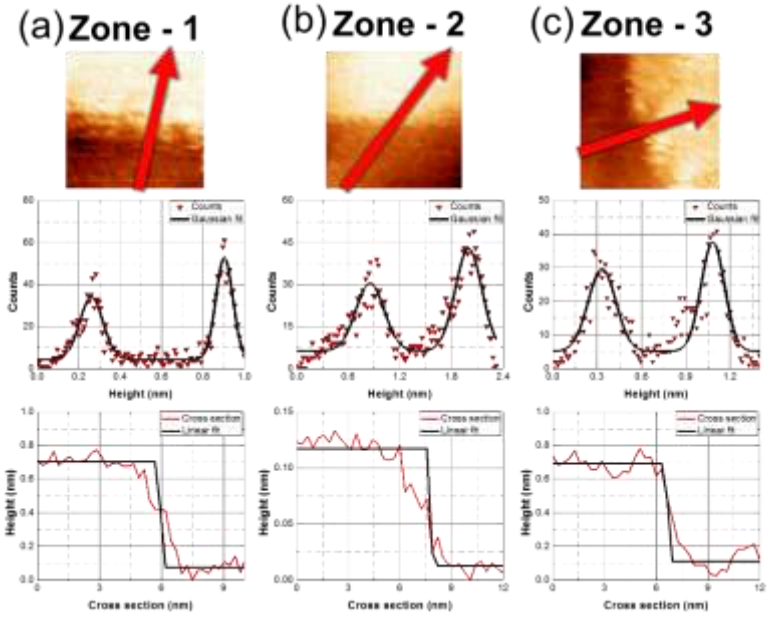

Figure 4.20 : Chosen zones from Figure 4.19 STM topography image in the first row. Graphs on the second row are histogram and the third row are line-scan analysis results.

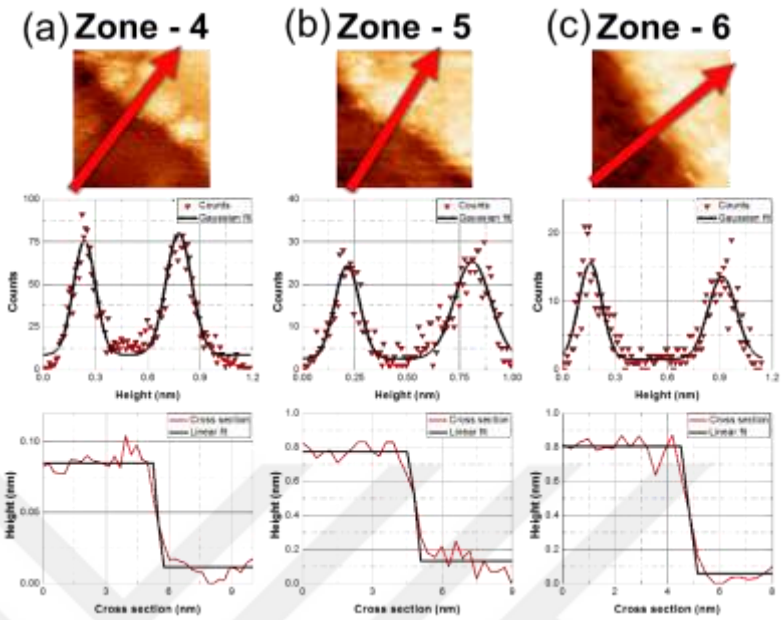

Figure 4.21 : Chosen zones from Figure 4.19 STM topography image in the first row. Graphs on the second row are histogram and the third row are line-scan analysis results.

Table 4.5 : Step height analysis results of chosen zones as shown in Figure 4.20 and Figure 4.21. d_h and d_{cs} are measured step heights which were obtained by using histogram and cross section method respectively. d_{calc} is the expected distance between two copper planes. n is the number of layers between two corresponding copper planes. ε_h and ε_{cs} are error rates of histogram and cross section measurements.. Photon emission (PE) observations were also given in the rightmost column.

Zone	d_h (nm)	d_{cs} (nm)	d_{calc} (nm)	n	Facet	ε_h (%)	ε_{cs} (%)	PE
1	0,646	0,628	0,627	3	Cu(111)	3,1	0,2	Yes
2	1,150	1,047	1,086	4	Cu(100)	5,9	3,6	No
3	0,756	0,737	0,724	2	Cu(100)	4,4	1,7	No
4	0,540	0,583	0,628	3	Cu(111)	14	7,1	Yes
5	0,605	0,315	0,628	3	Cu(111)	3,5	2,3	Yes
6	0,761	0,749	0,836	4	Cu(111)	9	10	Yes

In Figure 4.19, six different zones were analysed in terms of photon emissivity. Similarly to Figure 4.17, particular emissive characteristics of the surface was seen again. Following the same steps of facet identification analysis, zone-1, zone-4, zone-5 and zone-6 correspond to Cu(111) faces where photon emission was observed. On the other hand,

zone-2 and zone-3 appeared as Cu(100) oriented facet where there was not photon radiative.

The results have indicated that not only the specimen material but also the crystal orientation of the substrate beneath graphene can be decisive on photon emission. Analysis results have revealed that photon emissive zones are corresponding to Cu(111) facets beneath graphene in contrast to Cu(100) and Cu(110) surfaces. It also has to be mentioned that only Cu(111) facets have free electron like surface states [29, 30]. It can be attributed to photon emissive surface plasmons can be generated on these facets in G/Cu system due to their specific surface charge density. We have observed emitted photons in optical (VIS) and near-infrared (NIR) range by using silicon diode photodetector. In addition, measured signals from the photodetector were converted to femtowatt from volts using (2.5). Based on our experimental results, we can attribute photon observation to two major mechanisms. The first one is; STM-tip injected local surface plasmon (LSP) emits photon at the edges of varying surface clusters as photon maps of Au/Mica and Au/Cr/Mica have shown. On the other hand, free electron like surface states forming between G/Cu may yield the occurrence of gap-plasmons of the tip-interface junction which is tend to decay into radiative SPPs along of the surface [6, 10]. However, proposed hypothesis needs further studies to explain photon emission mechanism of G/Cu interface system. Spectroscopic analysis could enlighten to identify properties of emitted photons.

5. CONCLUSION AND OUTLOOK

Graphene on copper prepared by using chemical vapour deposition (CVD) technique has been investigated with photon emission scanning tunnelling microscopy (pSTM) under ambient conditions. Tunnelling induced photon emission from the tip-graphene/Cu interface junction was observed. Based on the measurement results, emitted photons attributed to G/Cu interface states. We have claimed that the radiation was dependent on the local facet orientation of the polycrystalline copper foil which varies local charge characteristics. In addition, it was clearly revealed that graphene layer protected copper foil from being exposed to oxidisation by ambient conditions.

In this study, CVD grown graphene on copper sample was demonstrated as a nanoscopic scale light source. Collected photons were confined with the wavelength range of silicon photodetector diode was in VIS-NIR range. Simultaneously taken photon maps have appeared with well correlation with STM images. Furthermore, photon emission was homogenous on wide zones which was not varying scan direction dependently such as Au surface. To better understand this relation between photon map and topography, copper steps beneath graphene were analysed to see whether photon emission depends on the facet orientation. The analysis has revealed that photon emissive zones are corresponding to Cu(111) facets. On the other hand, non-emissive zones were stated as Cu(100), Cu(110) underneath graphene layer and surface impurities. These wrinkle kind surface impurities have also indicated that few layers of graphene. Certainly, increased number of graphene layers yields change in the dispersion at G/Cu interface as well.

Interpretation of photon emission which were observed only where G/Cu(111) systems exist can be structured as: The occurrence of the free electron like surface states forming between G/Cu may lead to the generation of gap plasmons at the tunnel junction, as known as LSPs. Thus, emitted photons along the surface were generated by these LSP decays into surface plasmon polaritons.

In conclusion, photon emission from metal-tunnel junction-graphene/metal system under ambient conditions was first reported in this study. It was clearly seen that crystal orientation of copper facets has a dominant role on this tunnelling induced luminescence from Graphene/Cu sample. Based on measurements, it was determined that the occurrence of free electron surface state of Cu(111) surfaces are decisive in photon emission.

REFERENCES

[1] **Coombs, J. H., Gimzewski, J. K., Reihl, B., Sass, J. K. & Schlittler, R. R.** (1988). Photon emission experiments with the scanning tunnelling microscope. *J. Microsc.* 152, 325–336.

[2] **Gimzewski, J. K., Sass, J. K., Schlitter, R. R. & Schott, J.** (1989). Enhanced Photon Emission in Scanning Tunnelling Microscopy. *Europhys. Lett.* 8, 435–440.

[3] **Barnes, W. L., Dereux, A. & Ebbesen, T. W.** (2003).Surface plasmon subwavelength optics. *Nature* 424, 824–30.

[4] **Taylor, P., Sambles, J. R., Bradbery, G. W. & Yang, F.** (2006). Optical excitation of surface plasmons : An introduction Optical excitation of surface plasmons : an introduction. 37–41.

[5] **Zeng, S., Baillargeat, D., Ho, H.-P. & Yong, K.-T.** (2014). Nanomaterials enhanced surface plasmon resonance for biological and chemical sensing applications. *Chem. Soc. Rev.* 43, 3426–52.

[6] **Divitt, S., Bharadwaj, P. & Novotny, L.** (2013). The role of gap plasmons in light emission from tunnel junctions. *Opt. Express* 21, 27452.

[7] **Lambe, J. & McCarthy, S.** (1976). Light emission from inelastic electron tunneling. *Phys. Rev. Lett.* 37, 923–925.

[8] **Laks, B. & Mills, D. L.** (1979). Photon emission from slightly roughened tunnel junctions. *Phys. Rev. B* 20, 4962–4980.

[9] **Adams, A. & Hansma, P. K.** (1981). Light emission from small metal particles and thin metal films excited by tunneling electrons. *Phys. Rev. B* 23, 3597–3601.

[10] **Uehara, Y., Kimura, Y., Ushioda, S. & Takeuchi, K.** (1992). Theory of Visible Light Emission from Scanning Tunneling Microscope. *Jpn. J. Appl. Phys.* 31, 2465–2469.

[11] **Zayats, A. V., Smolyaninov, I. I. & Maradudin, A. A.** (2005). Nano-optics of surface plasmon polaritons. *Phys. Rep.* 408, 131–314.

[12] **Persson, B. N. J. & Baratoff, A.** (1992). Theory of photon emisison in electron tunneling to metallic particles.pdf. 4–7.

[13] **Berndt, R., Gimzewski, J. & Johansson, P.** (1991). Inelastic tunneling excitation of tip-induced plasmon modes on noble-metal surfaces. *Phys. Rev. Lett.* 67, 3796–3799.

[14] **Horn, J., *et al.*** (1993). Studies of GaAs surfaces by scanning tunnelling induced photon emission. *Mater. Sci. Eng. B* 20, 183–185.

[15] **Kabakchiev, A., Kuhnke, K., Lutz, T. & Kern, K.** (2010). Electroluminescence from Individual Pentacene Nanocrystals. *ChemPhysChem* 11, 3412–3416.

[16] **Kuhnke, K., Kabakchiev, A., Lutz, T. & Kern, K.** (2012). Electroluminescence properties of organic nanostructures studied by scanning tunnelling microscopy. *Phys. Status Solidi* 249, 644–652.

[17] **Merino, P., Große, C., Rosławska, A., Kuhnke, K. & Kern, K.** (2015). Exciton dynamics of C60-based single-photon emitters explored by Hanbury Brown-Twiss scanning tunnelling microscopy. *Nat. Commun.* 6, 8461.

[18] **Johansson, P., Hoffmann, G. & Berndt, R.** (2002). Light emission from Na/Cu(111) induced by a scanning tunneling microscope. *Phys. Rev. B* 66, 245415.

[19] **Beams, R., Bharadwaj, P. & Novotny, L.** (2014). Electroluminescence from graphene excited by electron tunneling. *Nanotechnology* 25, 55206.

[20] **Chen, C.-F. *et. al.*** (2011)**..** Controlling inelastic light scattering quantum pathways in graphene. *Nature* 471, 617–620.

[21] **Bethune, D. S. *et. al.*** (1993). Cobalt-catalysed growth of carbon nanotubes with single-atomic-layer walls. *Nature* 363, 605–607.

[22] **Kroto, H. W., Heath, J. R., O'Brien, S. C., Curl, R. F. & Smalley, R. E.** (1985). C 60: buckminsterfullerene. *Nature* 318, 162.

[23] **Wallace, P. R.** (1947). The band theory of graphite. *Phys. Rev.* 71, 622–634.

[24] **Castro Neto, A. H., Guinea, F., Peres, N. M. R., Novoselov, K. S. & Geim, A. K.** (2009). The electronic properties of graphene. *Rev. Mod. Phys.* 81, 109–162.

[25] **Chen, J. H., Jang, C., Xiao, S., Ishigami, M. & Fuhrer, M. S.** (2008). Intrinsic and extrinsic performance limits of graphene devices on SiO2. *Nat. Nanotechnol.* 3, 206–209.

[26] **Nair, R. R. *et al.*** (2008). Fine Structure Constant Defines Visual Transperency of Graphene. *Science (80-.).* 320, 2008.

[27] **Chen, S. *et al.*** (2011). Oxidation resistance of graphene-coated Cu and Cu/Ni alloy. *ACS Nano* 5, 1321–1327.

[28] **Tao, X. *et al.*** (2009). Influence of a dielectric layer on photon emission induced by a scanning tunneling microscope. *J. Chem. Phys.* 130.

[29] **Crommie, M. F., Lutz, C. P. & Eigler, D. M.** (1993). Imaging standing waves in a two-dimensional electron gas. *Nature* 363, 524.

[30] **Bürgi, L., Knorr, N., Brune, H., Schneider, M. A. & Kern, K.** (2002). Two-dimensional electron gas at noble-metal surfaces. *Appl. Phys. A Mater. Sci. Process.* 75, 141–145.

[31] **Shockley, W.** (1939). On the surface states associated with a periodic potential. *Phys. Rev.* 56, 317–323.

[32] **Schubert, K. *et al.*** (2012). Momentum-resolved electron dynamics of image-potential states on Cu and Ag surfaces. *Phys. Rev. B - Condens. Matter Mater. Phys.* 85, 1–9.

[33] **Kittel, C.** (2004). Reciprocal Lattice, *Introduction to Solid State Physics*, (pp. 43). John Wiley and Sons Inc.

[34] **Novoselov, K. S. *et al.*** (2012). REVIEW A roadmap for graphene. *Nature* 490, 192–200.

[35] **Li, X.** (2012). Large-Area Synthesis of High-Quality. 1312.

[36] **Bhaviripudi, S., Jia, X., Dresselhaus, M. S. & Kong, J.** (2010). Role of kinetic factors in chemical vapor deposition synthesis of uniform large area graphene using copper catalyst. *Nano Lett.* 10, 4128–4133.

[37] **Celebi, K. *et al.*** (2013). Evolutionary kinetics of graphene formation on copper. *Nano Lett.* 13, 967–974.

[38] **Liang, X. *et al.*** (2011). Toward clean and crackless transfer of graphene. *ACS Nano* 5, 9144–9153.

[39] **Walmsley, D. G., Tan, T. S. & Dawson, P.** (2004). Light emission from gold and silver thin films in a scanning tunneling microscope: Role of contamination and interpretation of grain structure in photon maps. *Surf. Sci.* 572, 497–520.

[40] **Aizpurua, J., Apell, S. & Berndt, R.** (2000). Role of tip shape in light emission from the scanning tunneling microscope. *Phys. Rev. B* 62, 2065–2073.

[41] **Smekal, A.** (1928) Zur Quantentheorie der Streuung und Dispersion. *Naturwissenschaften* 16, 612–613.

[42] **Raman, C. V. & Krishnan, K. S.** (1928). A New Type of Secondary Radiation. *Nature* 121, 501–502.

[43] **Gardiner, D. J.** (1989) *Practical Raman Spectroscopy*, 1–12, Springer Berlin Heidelberg.

[44] **Binnig, G. & Rohrer, H.** (1982). Scanning tunneling microscopy. *Surf. Sci.* 126, 236–244.

[45] **Schrödinger, E.** (1926). An undulatory theory of the mechanics of atoms and molecules. *Phys. Rev.* 28, 1049–1070.

[46] **Chen, C. J.** (1993). *Introduction to Scanning Tunneling Microscopy.* New York: Oxford University Press

[47] **Binnig, G., Rohrer, H., Gerber, C. & Weibel, E.** (1983). 7x7 Reconstruction on Si(111) Resolved in Real Space. *Phys. Rev. Lett.* 50, 120–123.

[48] **Binnig, G. & Quate, C. F.** (1986). Atomic force microscope, *Phys. Rev. Lett.* 9, 56.

[49] **Demtröder, W.,** (2006), Interaction Between Two Neutral Atoms, *Molecular Physics: Theoretical Principles and Experimental Methods.* (pp. 116-119). Weinheim: Wiley-VCH.

[50] **Pitzer, K. S.,** (1968), Chemical physics, *Science*, 160, 1330.

[51] **Kamber, U.,** (2017), *Formation of dendritic silicon-oxide structures during chemical vapor deposition growth of graphene on copper*. (MSc. Thesis). Istanbul Technical University, Graduate School of Science, Engineering and Technology, Istanbul.

[52] **Tamer, M. S.,** (2013). *Design and construction of a setup for the detection of tunneling induced photons in a scanning tunneling microscope and an application on gold surfaces*. (MSc. Thesis). Istanbul Technical University, Graduate School of Science, Engineering and Technology, Istanbul.

[53] **Thorlabs Femtowatt Photoreceiver PDF10x Operation Manual**. (2017). *Retrieved April 27, 2017, from http://www.thorlabs.de/thorcat/16000/PDF10A_M-Manual.pdf*.

[54] **Ferrari, A. C. *et al.*** (2006). Raman spectrum of graphene and graphene layers. *Phys. Rev. Lett.* 97, 1–4.

[55] **Malard, L. M., Pimenta, M. A., Dresselhaus, G. & Dresselhaus, M. S.** (2009). Raman spectroscopy in graphene. *Phys. Rep.* 473, 51–87.

[56] **Rasool, H. I. *et al.*** (2011). Continuity of graphene on polycrystalline copper. *Nano Lett.* 11, 251–256.

[57] **Rasool, H. I. *et al.*** (2011). Atomic-scale characterization of graphene grown on copper (100) Single Crystals. *J. Am. Chem. Soc.* 133, 12536–12543.

[58] **Yildiz, D. & Gürlü, O.** (2016). Apparent corrugation variations on moiré patterns on highly oriented pyrolytic graphite. *Mater. Today Commun.* 8, 72–78.

[59] **Gonzalez-Herrero, H. *et al.*** (2016). Graphene Tunable Transparency to Tunneling Electrons: A Direct Tool to Measure the Local Coupling. *ACS Nano* 10, 5131–5144.

[60] **Lalmi, B. *et al.*** (2014). Flower-shaped domains and wrinkles in trilayer epitaxial graphene on silicon carbide. *Sci. Rep.* 4, 4066.

[61] **Björkman, T. *et al.*** (2013). Defects in bilayer silica and graphene: common trends in diverse hexagonal two-dimensional systems. *Sci. Rep.* 3, 3482.

APPENDICES

APPENDIX A: User manual for pSTM applications.

APPENDIX A

1- Chosen sample is mounted on STM head.
2- Using stage system which has five degrees of freedom, collimator-lens system is focused on the tip-sample junction area.
3- The system electronic is switched on.
4- System software is started. (To avoid software based errors, this step is always done after switching on the system electronics.)
    a. Label and file address of the measurements are entered via system software.
    b. Tunnelling parameters are set via system software.
    c. STM tip is approached to the surface via software with eye control through lens-collimator system.
5- Lens-collimator system and photodetector are connected via a fibreoptic cable.
6- Windows of the dark box are closed for external light noise isolation.
7- Photodetector is plugged in, switched on and checked using oscilloscope whether receiving signal or not.
8- When the system is read for measurements;
    a. Using auto approach mode, tunnelling process is begun.
    b. Surface scan is started for the surface characterisation step.
    c. If the tunnel current and scanned surface are satisfying, photon map channel is switched on as well.
    d. Tunnelling current and bias voltage are increased.
        i. Tunnelling parameters are increased step by step to avoid the risk of tip-crash, tip deformation etc.
        ii. Oscilloscope has to be checked continuously to see possible abnormalities in the tunnel current.
9- Simultaneously taken photon map is checked from oscillator showing real-time junction and emission characteristics while surface is being scanned.
10- When measurements are done;
    a. Tunnelling current and bias voltage are decreased
    b. Photon Map channel is switched off.
    c. Same surface is scanned with decreased tunnelling parameters to see if the surface or the tip is manipulated during measurements.
    d. Using retract button, the tip is taken out from tunnelling junction.
    e. The tip is retracted with course mode for safety reasons until far enough from the surface.
    f. System software is closed.
11- Photodetector is switched off.
12- System electronic is switched off.
13- Optic table is landed on the legs.
14- Windows of the dark box are opened.
15- Fibreoptic cable is disassembled.
16- The sample is taken out from the holder.
17- The holder is stored in its protection box.

CURRICULUM VITAE

Name Surname **:** Hakkı Tunç Çiftçi

Place and Date of Birth **:** Ankara, 06.08.1990

e-mail **:** ciftciha@itu.edu.tr

tuncciftci@gmail.com

EDUCATION **:**

- **B.Sc.** **:** 2015, Istanbul Technical University, Faculty of Science and Literature, Physics Engineering
- **M.Sc.** **:** 2017, Istanbul Technical University, Graduate School of Science Engineering and Technology, Physics Engineering

PUBLICATIONS AND PRESENTATIONS ON THE THESIS:

- Çiftçi H. T., Zengin B., Kamber U., Kıncal C., Yıldız D., Gürlü O., 2015: Optical emission and absorption characteristics of graphene on copper in a tunnel junction. 79th Annual Meeting of the DPG and DPG Spring Meeting, March, Berlin, Germany.

- Zengin B., Çiftçi H. T. and Gürlü O., 2015: Role of the tip in photon emission from Au surfaces in Scanning Tunnelling Microscopy. 79th Annual Meeting of the DPG and DPG Spring Meeting, March, Berlin, Germany.

- Çiftçi H. T., Zengin B., Kamber U., Kıncal C., Yıldız D. and Gürlü O., 2016: Tunneling electron induced photon emission from graphene/copper interface. NanoTR12, 12th Nanoscience and Nanotechnology Conference, Kocaeli, Turkey.

- Zengin B., Çiftçi H. T. and Gürlü O., 2016: Tip dependence of tunnelling induced photon emission from Au and Au/Cr surfaces. NanoTR12, 12th Nanoscience and Nanotechnology Conference, Kocaeli, Turkey.

- Çiftçi H. T., Zengin B., Kamber U., Kıncal C., Yıldız D. and Gürlü O., 2016: Photon emission from graphene/copper interface in a tunnel junction. GRM2016, 2016 Graphene & Related Materials Conference, Ankara, Turkey.